Segmenting and Modeling the Human Airway with Voicing or Breathing Disorders

By

Mukund Gupta

Thesis

Submitted to the Faculty of the

Graduate School of Vanderbilt University

in partial fulfillment of the requirements

for the degree of

Master of Science

In

Mechanical Engineering

May 10, 2024

Nashville, Tennessee

Approved:

Haoxiang Luo, Ph.D.

Leon Bellan, Ph.D.

To my family

ACKNOWLEDGMENTS

I would like to express immense gratitude to my adviser Professor Haoxiang Luo who allowed me to work on this thesis, guided me throughout my journey at Vanderbilt and enabled me to become a better researcher and a better person. This thesis would not have been possible without his support, guidance, and help. I really appreciate the time he invested in ensuring that this thesis attains its current form after multiple drafts. The learnings and teachings he provided will be carried out by me in my work and in any assignments I take charge of in the future.

I would also like to thank Professor Leon Bellan for agreeing to be a part of my thesis committee. I have learned a lot from him by being a TA for the course ES140x: Introduction to Engineering Module (Mechanical Engineering), where I learned how to make a complex topic of sound compression in five weeks yet interesting for the students. His approach to tackling problems is truly remarkable, and I hope to use my learnings under his supervision to tackle the complex problems that I will encounter in my job when dealing with acoustic problems.

I would also like to thank Dr. Yike Li for agreeing to be a part of my thesis committee and for supporting me during the last year. Dr. David Kent and his consideration and belief that I would be able to carry out this project meant a lot to me. I really appreciate his willingness to help whenever I was stuck with doubts on anatomy, tissue properties, or needing resources to understand the problem better. The financial support offered by Dr. David Kent and him over the last summer allowed me to work stress-free on developing a model for simulating the Ansa cervicalis stimulation in treating obstructive sleep apnea.

I would also like to thank my parents, younger brother, and my grandmother for their constant support and encouragement throughout my academic journey.

Lastly, I would like to thank my friends in Nashville who became like my family. Pawan, Aditya, Mamatha, and Paridhi, this journey would not have been possible without you. I would also like to thank all the friends I made during my time at Vanderbilt. I have learned a lot from all of you that I will carry forward in my life.

TABLE OF CONTENTS

LIST OF TABLES

LIST OF FIGURES

CHAPTER 1

Background Introduction

1.1 Upper Airway Disease

The upper airway is that part of the respiratory system between the nostrils or lips and the trachea and is an important contributor to overall respiratory resistance and to conditioning of inspired air. It comprises the nasal cavities, oral cavity, pharynx, and larynx, with the pharynx further divided into the nasopharynx, oropharynx, and hypopharynx. The larynx, in turn, is categorized into the supraglottis, glottis, and subglottis, based on their proximity to the vocal cords (glottis). The supraglottis encompasses the epiglottis, arytenoids, aryepiglottic folds, false cords, and ventricles, while the subglottis extends from just beneath the vocal cords' free edge to the lower margin of the cricoid cartilage. The most important functions of the upper airway include air warming and humidification, pathways for olfaction, coordination of ventilation with swallowing and protection from aspiration of food, primary defense of infection, and especially for humans, speech. Evolution of speech has required laryngeal motility, leaving the human upper airway reliant on surrounding soft tissues for support and thus vulnerable to collapse [1]. All of these functions are controlled by highly evolved neuromuscular systems under both voluntary and involuntary control [1]. These systems work efficiently in health but can come into conflict in diseases of the lungs and chest wall, and the upper airway in particular [1–3].

Obstruction within any of these structures, ranging from constriction to complete blockage, can compromise ventilation, necessitating prompt recognition and intervention by healthcare professionals [4]. Noisy breathing, characterized as 'stertor' or 'stridor,' serves as a key clinical indicator [4]. Stertor refers to noisy breathing above the larynx, whereas stridor occurs at or below the larynx. Stridor can further manifest as inspiratory (supraglottic level), expiratory (glottic level), or biphasic (subglottic or tracheal level). Upper airway obstruction may be partial or complete. A partial obstruction can be chronic or acute. Failure to address upper airway obstruction promptly can lead to severe long-term consequences or even fatalities[4]. In health and during wakefulness, common coordinated activities of this complex neuromuscular control system include coughs, hiccups, aspiration recovery, vomiting, and sneezing [1].

Vocal Cord Dysfunction, often presenting as an asthma mimic, is believed to be intricately linked to the coordinated neural regulation of respiratory phases and vocal cord movements[5]. Conversely, the maintenance of upper airway patency assumes paramount importance during sleep, as failure in this regard can precipitate obstructive sleep apnea and its associated complications. Sleep represents a period of heightened vulnerability, characterized by a dampening of protective upper airway reflexes [1], rendering the upper airway

susceptible to collapse[1]. Emerging evidence indicates that the pathogenesis of OSA involves a multifaceted interplay among various factors, including upper airway anatomy, pharyngeal dilator motor control, and ventilatory control instability, notably loop gain [1], either individually or in concert. Moreover, the relative contribution of each factor to the development of OSA varies significantly among affected individuals [6], underscoring the necessity of elucidating the underlying mechanisms of Obstructive Sleep Apnea (OSA) in each patient to facilitate tailored therapeutic interventions [6]. The goal of this thesis is to evaluate a couple of methods used for treatment of unilateral vocal fold paralysis, a type of vocal cord disorder and OSA. For unilateral vocal fold paralysis, type 1 thyroplasty is used as a means of treatment whereas for OSA, ansa cervicalis stimulation is used.

1.2 Unilateral Vocal Fold Paralysis (UVFP)

Unilateral Vocal Fold Paralysis (UVFP) is a condition that occurs when one of the vocal folds is unable to move properly due to nerve damage or other causes. This can lead to voice changes, difficulty in speaking, and swallowing difficulties. Vocal folds are a pair of highly specialized tissues situated within the larynx which vibrate to produce noise when adducted into glottal controlled airflow [7]. UVFP is a relatively common condition with a reported incidence rate of 5 per every 100,000 annually [8]. It can occur at any age, but is more common in older adults, especially those with a history of throat or neck surgery, trauma, or neurological conditions [9]. Diagnosis of UVFP is typically made by an ear, nose, and throat (ENT) specialist or a speech-language pathologist (SLP), who may perform a laryngoscopy or other diagnostic tests to assess the vocal fold movement. Treatment for UVFP depends on the severity and duration of the paralysis, as well as the individual's goals and preferences. Non-surgical treatments such as voice therapy, respiratory training, and behavioral modifications may be effective in some cases. Surgical treatments such as injection laryngoplasty, medialization laryngoplasty, or reinnervation procedures may be necessary in more severe cases. UVFP can have a significant impact on a person's quality of life, and early diagnosis and treatment are important to improve outcomes and prevent complications.

Implants are needed to treat unilateral vocal fold paralysis when the vocal fold is unable to move properly due to nerve damage or other causes. When the vocal fold is paralyzed, it may not be able to vibrate properly during speech or singing, resulting in voice changes, difficulty speaking, and swallowing difficulties. Implants can be used to augment the paralyzed vocal fold and improve its movement and function, helping to restore normal voice production [10–12]. Mattioli et.al [13] reported that injection laryngoplasty, which involves the injection of a material such as hyaluronic acid or collagen into the paralyzed vocal fold, can be an effective treatment for unilateral vocal fold paralysis. The study found that the treatment improved the voice quality and swallowing function in patients with unilateral vocal fold paralysis, with minimal complications. Another study reported that medialization laryngoplasty, which involves the placement of a permanent or temporary

implant to push the paralyzed vocal fold towards the midline, can be a safe and effective treatment for unilateral vocal fold paralysis [14]. The study found that the treatment improved the voice quality and reduced the swallowing difficulties in most patients, with a low rate of complications. Type 1 thyroplasty is a surgical procedure used to treat unilateral vocal fold paralysis by medializing the paralyzed vocal fold. This procedure involves making an incision in the neck and inserting a silicone implant or other material into the thyroid cartilage to push the paralyzed vocal fold towards the midline. Research has shown that type 1 thyroplasty can be a safe and effective treatment option for patients with unilateral vocal fold paralysis. Varadarajan et. al [15] reported that type 1 thyroplasty improved voice quality and reduced breathiness in patients with unilateral vocal fold paralysis. The study also found that the procedure had a low rate of complications, and most patients reported improved quality of life after the surgery. Others reported similar findings, with type 1 thyroplasty resulting in improved voice quality and reduced breathiness in patients with unilateral vocal fold paralysis [16]. The study also found that the procedure had a low rate of complications and was well-tolerated by most patients.[14–17].

Developing novel computational FEM models is critical to understanding and solving the UVFP problem through type-1 thyroplasty as it provides surgeons with a better understanding of anatomy and improved surgical planning. Li et al. developed a rabbit vocal fold model tailored to individual subjects, utilizing MRI scans taken under various surgical conditions affecting vocal fold approximation[7]. These conditions included both non-approximated (NA) and others. By analyzing these scans, particularly those from the NA condition, precise cartilage displacement data was extracted, and integrated as a boundary condition into their Finite Element Method (FEM) model. This integration enabled them to simulate vocal fold deformation and subsequent structural stiffening accurately. Notably, unlike prior studies, their FEM model incorporates subject-specific anatomy and cartilage displacement derived directly from MRI data. Additionally, while previous research primarily focused on normal healthy vocal fold adduction, characterized by symmetrical vibration on both sides, their study introduces a simulated Unilateral Vocal Fold Paralysis (sUVFP) condition. Under sUVFP, vocal folds are asymmetrically approximated, leading to varied structural stiffening between the two sides. A part of this thesis highlights the computational pipeline followed to get the FEM model from the MRI images and shows the final FEM model obtained from the image segmentation. Three New Zealand rabbit larynx are segmented for three different conditions: rest, one side suture, and one side suture and one side.

1.3 Obstructive Sleep Apnea

This thesis also delved into obstructive sleep apnea, a prevalent medical condition characterized by recurrent upper airway collapse and its associated consequences, impacting nearly half a billion individuals globally [18,19]. The gold standard for mitigating the health effects of OSA remains positive airway pressure, which

continues to be the primary treatment modality [20,21]. However, a significant proportion of patients, ranging from 39% to 50%, encounter difficulties in adhering to this therapy[22]. While surgical interventions can effectively alleviate the burden of OSA in specific patients, success rates vary. Despite advancements in hypoglossal nerve stimulation (HNS), its application is limited, and a considerable number of eligible patients continue to experience inadequate relief [23]. HNS functions by widening the airway at multiple levels, primarily by repositioning the tongue downwards, with promising outcomes attributed to mechanical connections between the tongue and other pharyngeal structures, including the soft palate[21]. Some individuals do not respond optimally to HNS, possibly due to a point of diminishing returns where increased electrical stimulation fails to completely alleviate airway obstruction [22]. This indicates localized and insufficient effects of HNS for certain recipients, even with rigorous selection criteria. Additionally, excessive protrusion of the tongue during HNS may lead to discomfort, tongue abrasion, and dry mouth [22]. The pharynx possesses ventral attachments to movable structures, such as the mandible and hyoid bone, as well as caudal attachments to the thyroid cartilage, enabling dynamic adjustments in shape and tension bidirectionally. A well-established technique involves caudal tracheal traction, which unfolds and stretches the pharyngeal walls lengthwise, reducing compliance and alleviating peripharyngeal tissue pressure to enhance pharyngeal openness[23].

Humans exhibit significant rostro-caudal movement of the hyolaryngeal complex due to adaptations for speech and swallowing, facilitated in part by cervical strap muscles [22]. Previous experiments on animals with less mobile larynges demonstrated significant enhancements in airway collapsibility and reductions in peripharyngeal tissue pressure through infra-hyoid muscle traction and electrical stimulation[21] . To address these limitations associated with HNS, Kent et al. proposed a new surgical technique, Ansa Cervicalis Stimulation [22,23]. The idea behind using ansa cervicalis stimulation stems from the fact that the sternothyroid muscle would contract via ansa cervicalis stimulation (ACS) leading to increased pharyngeal patency in humans with OSA. Kent et. al. found substantial increases in maximum inspiratory airflow and highlighted the potential role of ACS as a novel respiratory neurostimulation (RNS) strategy for treating OSA[22].

1.4 Computational Modeling for Treating Airway Disease

Despite the well-recognized consequences of various upper airway diseases, most of the treatments remain unsatisfactory. Therapeutic strategies are complicated by often poor adherence in the case of continuous positive airway pressure or the highly variable efficacy in the case of many upper airway surgeries. Computational models of the upper airway using finite element analysis to simulate the effects of various anatomic and physiologic manipulations on pharyngeal mechanics could be helpful in predicting surgical success. Because surgical techniques result in permanent anatomic changes, without any need for patient adherence once the procedure is completed, many investigators have sought methods to predict responsiveness to surgical therapy to maximize potential benefits on patient outcome. Many authors in the

literature have been using the technique of finite element analysis (FEA) to model the upper airway to allow the prediction of changes in pharyngeal mechanics after anatomic and physiologic manipulations[24]. Because of the complexity of the human upper airway, the lack of suitable animal models, and the lack of feasibility of human experiments to manipulate anatomy, many believe computational simulation may be the ideal technique with which to predict outcomes after upper airway manipulation[24–27]. Usage of FEM is predominant within the biomechanics community to identify and characterize the material properties as well as understand the complex interaction of various components to understand the upper airway mechanics. Others have suggested the usage of Computational Fluid Dynamics (CFD) and fluid structure interaction (FSI) to tackle the existing problems associated with upper airway modeling[7] . Recent works in our group[7,28–30] have used FEA and FSI to predict eigen modes of the stressed vocal folds using a non-stimulated cricothyroid suture approximation model to elicit sustained vocal fold phonation in rabbits and also validated the experimental observations. And similarly, authors have used 3D and 1D FSI to simulate the phonation of vocal folds for subject specific FEM models segmented using MRI images[28,29] .

CFD has also been used extensively to study various upper airway diseases as the CFD analysis is able to provide clear visualization and its results can cover the lack of information from experiments such as the flow properties and flow pattern generated inside the human upper airway. to study the critical airflow of the upper airway prior to conducting the surgery[31]. This makes CFD a vital and useful tool for predicting the various flow properties in the human upper airway by computationally solving flow equations[31] . Recent work by Faizal et. al. has summarized the application of CFD studies for various upper airway diseases. Many works have focused on using computational modeling for OSA as computational models can provide valuable insight into the functioning of the tongue and the influence of the airway dynamics on its motion[31]. These models are mathematical representations of anatomy, with geometrical descriptions of the tissues being coupled to models that predict the response of the tissues to forces that act upon them. Provided that a representative model can be constructed, and the surrounding environmental conditions described with sufficient accuracy, these models may enhance understanding of the influence of various conditions which may not necessarily be able to be investigated experimentally. In order to produce such a model, an accurate description of the geometry of the human upper airway must be constructed. Furthermore, the underlying histology of the various tissues should be considered, and their influence accounted for within the model. The models that govern the response of the tissues are often directly correlated to experimental analysis performed at the macro- and microscopic levels[32,33] . Through this thesis, an effort has been made to develop computational models for treating UVFP with type 1 thyroplasty and OSA with Ansa Cervicalis Stimulation to help surgeons with pre-surgery planning and in deriving better insights of the patient's anatomy to improve surgical outcomes.

CHAPTER 2

Image Segmentation for Unilateral Vocal Fold Paralysis

2.1 Research Significance and Objectives

The work presented in this chapter is a part of PhonoSim, which our research group has developed. PhonoSim uses pre-intervention MRI scans and the finite-element method (FEM) to determine optimal implant placement for type I thyroplasty thus enabling model informed surgery. The subject-specific rabbit vocal fold models were constructed based on the excised MRI scans at different surgical vocal fold approximation conditions. A simulated UVFP condition (sUVFP) was considered, in which the two vocal folds were asymmetrically approximated, and the corresponding FEM model was built that has different structural stiffening due to deformation between the two sides. This model allows us to study the effect of the asymmetric adduction on the vocal fold vibration without having to make ad hoc assumptions of different material stiffness properties for the two sides. Compared with previous studies, our FEM model incorporates the subject-specific anatomy and the displacement of the cartilage from the MRI data. Furthermore, previous works predominantly focused on normal healthy vocal fold adduction, with the two sides producing symmetrical vibration. Due to the subject specific nature of the segmented images from the MRI data, they can be used to perform eigenvalue analysis to determine the implant position for type 1 thyroplasty and help with pre-surgery planning to obtain better surgical outcomes. To be able to computationally model this problem of treating UVFP with type 1 thyroplasty accurately, specifying different material properties to the various parts that constitute the vocal fold of the patient as well as applying appropriate boundary conditions on specific surfaces is essential. Segmentation helps in this aspect by defining well defined 3D volumes with clear and distinct boundaries which can later be imported to COMSOL or an appropriate FEA software, where applying material properties and as well as meshing will be convenient. Through this work, three samples in three different configurations were segmented and used in helping the surgeons with implant. Model-informed implant surgeries achieved clinically meaningful adduction in all 6 instances as well as reduced variations in the implant location relative to the model-predicted position[30]. This is a significant improvement from the existing methods which involves almost two-thirds of laryngologists using Silastic® implants to medialize the vocal fold, with implant size, shape, and location determined experientially as post-surgical complications arising from this procedure (extrusion, migration, resizing) necessitate revision in 4.5–16% of patients.

2.2 Experimental Collaboration

This research was carried out in collaboration with Dr. Bernard Rousseau's group at the University of

Pittsburgh. All the experimental procedures were carried out at the Department of Laboratory Animal Research, University of Pittsburgh, which is accredited by AAALAC. The study adhered to the guidelines outlined in the "Guide for the Care and Use of Laboratory Animals" as well as the Animal Welfare Regulations, ensuring compliance with ethical standards. Three New Zealand white rabbits were included in the study. The rabbit model is well-established in phonation literature because of its comparable anatomical, biological, and biomechanical vocal fold properties with those in humans[7,28,30] .

The rabbits were administered sedatives consisting of 20 mg/kg ketamine and 0.125 mg/kg dexmedetomidine through intramuscular injection. To sustain anesthesia as necessary, a continuous rate infusion of 350 μg/kg/min ketamine and 1.65 μg/kg/min dexmedetomidine was delivered intravenously through a 27G catheter into the marginal vein. Vital signs including heart rate, respiratory rate, temperature, and oxygen partial pressure were meticulously monitored throughout the procedure. In vivo phonation studies were conducted, the neck and chest of anesthetized rabbits were prepared by shaving, and the rabbit was positioned in a supine posture. A longitudinal skin incision was performed from the sternum to the submentum, followed by dissection of the fascia and muscle along the midline to expose the larynx and trachea. The trachea was divided, and an uncuffed endotracheal tube was carefully inserted into the upper airway to facilitate direct oxygen delivery to the lungs. Additionally, a cuffed endotracheal tube was positioned in the upper region of the trachea to deliver humidified airflow at a temperature of 37 °C to the subglottic area. Utilizing a pediatric laryngoscope via oral insertion allowed for the suspension of the larynx and visualization of the vocal folds. Furthermore, a combination of humidified airflow and cricothyroid suture approximation techniques were employed. The cricothyroid suture approximation procedure was conducted with slight adjustments to achieve specific laryngeal conditions, including non-approximated (NA), healthy phonation (HP), and asymmetric vocal fold closure characteristic of unilateral vocal fold paralysis (UVFP) conditions (sUVFP). Each condition was systematically executed to ensure comprehensive assessment within each larynx.

For the NA condition, high-speed video endoscopy (HSV) of the vocal folds was captured in a neutral resting position. In the HP condition, bilateral Vicryl 5.0 sutures (Ethicon) were utilized to suture the cricoid cartilage to the thyroid cartilage. This intervention resulted in the lengthening of both vocal folds, facilitating their medial approximation. In the sUVFP condition, sutures were selectively removed from the right side of the larynx. This action released tension from the right vocal fold, leading to a characteristic "floppy" appearance indicative of UVFP. Larynges were collected for MRI analysis from animals that had not undergone any previous interventions. The excised larynges were scanned under the following experimental conditions: non-approximated (NA), healthy phonation (HP), and simulated unilateral vocal fold paralysis (sUVFP). The excised larynges were placed within a 10 mL syringe filled with perfluorocarbon oil, and images were acquired using a Bruker AV3HD 11.7 tesla/89 mm vertical-bore micro-imaging system equipped with a 40-

mm micro2.5 set capable of 1500 mT/m and ParaVision 6.0.1 software (Bruker Biospin). Three-dimensional T2-weighted images were obtained with an isotropic resolution of 60 μ using a fast spin-echo sequence, employing the following parameters: repetition time (TR) of 1000 ms, echo time (TE) of 28 ms, matrix size of 256 × 384 × 286, field-of-view of 16 × 16 mm, and a RARE (Rapid Acquisition with Relaxation Enhancement) factor of 8.

Three different vocal fold configurations were established for the current ex vivo study. The first configuration is the resting condition that was characterized by both vocal folds being positioned in an abducted manner within the non-innervated larynx. The second configuration involved surgical using injection laryngoplasty on one side. In contrast, the three-configuration representing type I thyroplasty configuration involved the insertion of an implant on one side of the larynx and surgical using injection laryngoplasty on one side, leading to a modification in the positioning of the vocal fold on that particular side.

2.3 Segmentation and Mesh Generation

For the reconstruction of the UVFP from imaging data, this work builds on an existing work carried out in the author's research group[7] . Here, three different New Zealand rabbit larynges were scanned ex vivo using MRI, and then the images were segmented manually. The following structural components were considered for model reconstruction: cricoid cartilage, thyroid cartilage, arytenoid cartilages, and soft tissue (vocal fold body and cover). These components are shown in figure 1.1, where the green color corresponds to the arytenoid cartilage, the red color corresponds to the cricoid cartilage, and the cyan color corresponds to the thyroid cartilage, the blue color corresponds to vocal fold body, and the yellow color corresponds to the vocal fold cover. These cartilages are critical for vocal fold positioning (e.g., adduction, abduction, and lengthening) prior to phonation and are therefore included in the segmentation process.

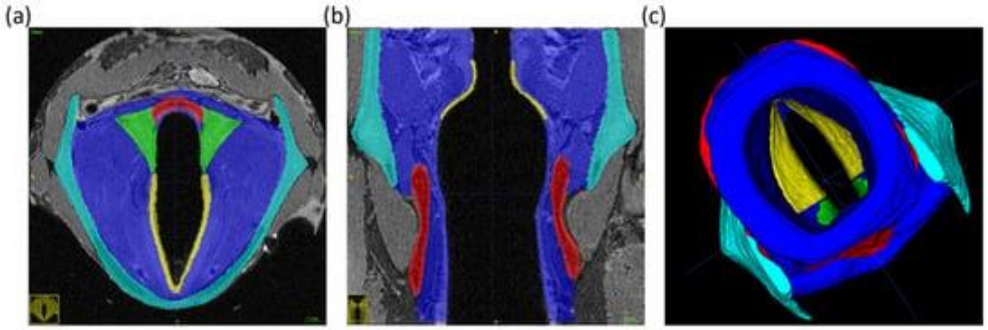

Figure 2.1: Vocal fold segmentation for sample 1. Green color represents the arytenoid cartilages; red color is

cricoid cartilage; cyan is the thyroid cartilage; blue is the vocal fold body; yellow is the vocal fold cover. (a) axial section; (b) coronal section; (c) 3D view from trachea [7].

Following manual segmentation, the surface mesh for each of these components was exported from the ITK-SNAP and then imported in Mesh Mixer (Autodesk, San Francisco, CA, USA) in order to mitigate the presence of uneven surfaces resulting from manual segmentation. However, this method yields individual surface mesh for each segmented component, leading to a lack of continuity between adjacent components such as the thyroid cartilage and the vocal fold body. Consequently, a thin gap may exist between these components' respective meshes. To address this issue, a holistic or unified surface mesh for the entire larynx was produced using ITK-SNAP and was subsequently refined through smoothing techniques utilizing MESH Mixer. Subsequently, the smoothed surface mesh was imported into COMSOL Multiphysics to facilitate the generation of the overall solid body and the sequential creation of unstructured volume mesh. Specifically, a tetrahedron mesh consisting of 10 nodes per element was applied during this process. The delineation of distinct structural components within the comprehensive larynx mesh was important for subsequent finite-element method (FEM) simulations. This identification or registration process entailed a comparative analysis between the nodes of the unified larynx volume mesh and those of individual structural components, wherein a minimum distance criterion was employed to ascertain the assignment of nodes to specific components. Through this methodology, each node within the unified larynx mesh was delineated and assigned corresponding to individual structural components, as depicted in Figure 2.2a. Moreover, regions of particular importance, such as the vocal fold cover, undergo mesh refinement to ensure higher density, as illustrated in Figure 2.2b.

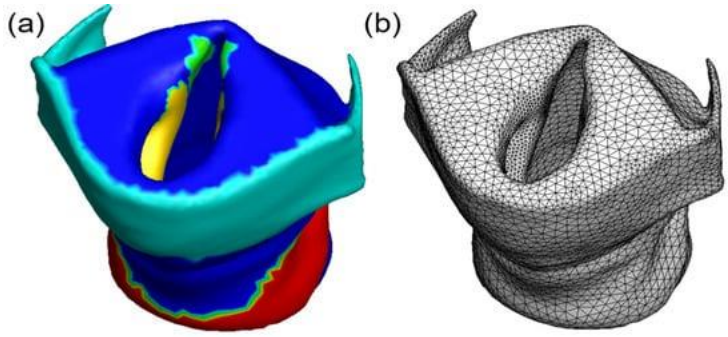

Figure 2.2: Reconstructed vocal fold from Sample 1 and the unified volume mesh.
(a) Reconstructed vocal fold. (b) Unstructured mesh for reconstructed vocal fold[7] .

2.4 Manual Segmentation Results for the UVFP cases

Manual segmentation of three different New Zealand rabbit's named Sample 20, 21, and 22 was carried out under three different configurations: rest configuration referred to as configuration 0, two side suture referred to as configuration 1, and one side suture and one side implant referred to as configuration 2. These models formed the basis of vocal fold adduction simulation as well as FSI simulation carried out and presented in the recent work carried out by Li et. al. in our group which describes the entire process in more detail[7] . To achieve vocal fold approximation, a laser-cut silastic implant was surgically inserted into the vocal fold, as illustrated in Figure 2.3 (c). This procedure was conducted using either a positioning approach based on anatomical landmarks scaled from the human larynx or a computationally guided position derived from PhonoSim modeling. A simple cuboidal implant shape, with two different insertion depths as depicted in Figure 2.3 (c), was utilized for both groups. These silastic implants were manufactured from a single sheet through laser-cutting, employing 3D CAD designs to ensure precise sizing, with dimensions as indicated in Figure 2.3 (c). Notably, this fabrication technique resulted in an implant closely resembling commercially available Montgomery implants in appearance. The section will present the images of the results obtained from the manual segmentation of the samples. Figure 2.3 (a) represents the configuration 0 and Figure 2.3 (b) represents the configuration 2 with implant inserted. Figure 2.4 shows the ITK-SNAP window during the segmentation process with the axial, sattigal, and coronal plane view.

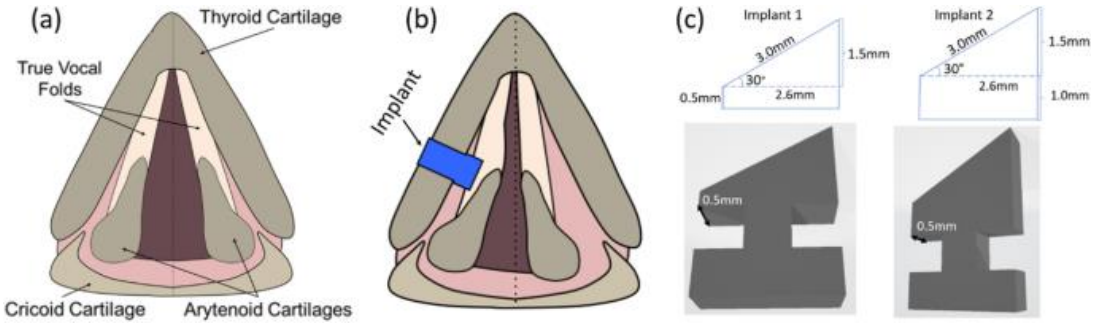

Figure 2.3: Schematic of type I thyroplasty surgery: (a) rest configuration, (b) implanted configuration, and (c) the customized implant with two different sizes[30] .

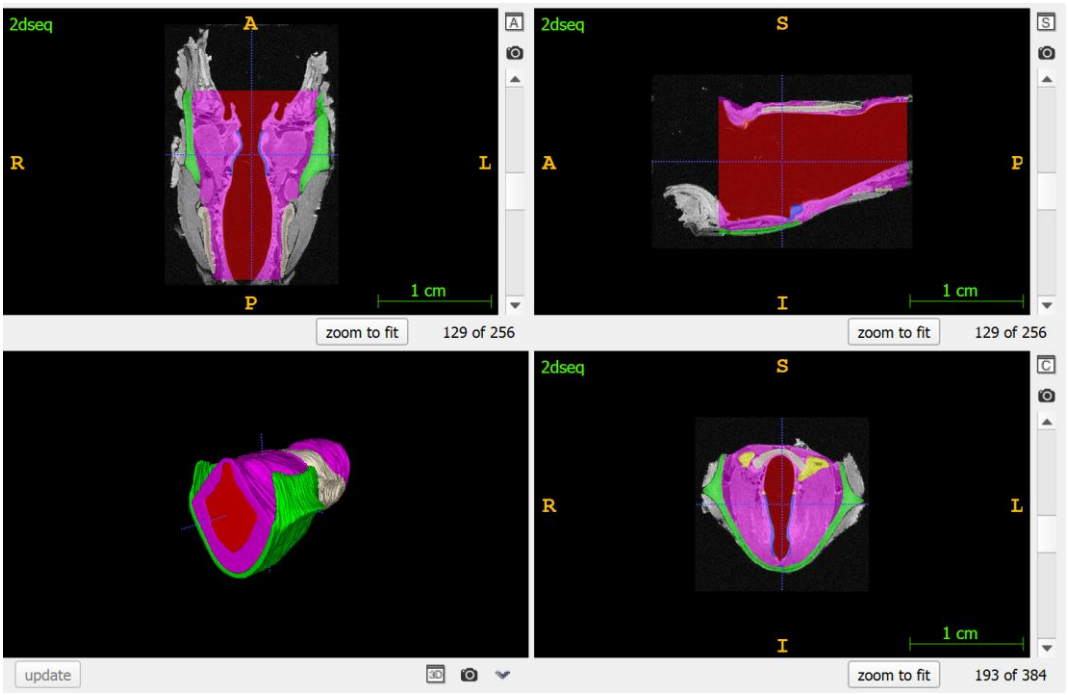

Figure 2.4: ITK-SNAP window during segmentation process.

2.4.1 Configuration 0

The rest configuration or configuration 0 represents the picture of the excised rabbit larynx before performing any surgical procedure. Figure 2.5 below shows the final segmented pharynx in three different views for samples 20, 21, and 22. Sample 20 corresponds to the first row, sample 21 corresponds to second row, and sample 22 corresponds to third row in the figure 2.5. The green color segment represents the thyroid cartilage, red color segment represents the air flow path, white color segment represents the cricoid cartilage, and the blue color segment represents the muscle containing the arytenoid cartilage and the vocal folds. The vocal folds and arytenoid cartilage are also segmented using purple and yellow color segments respectively but are housed within the muscle shown in blue. From the comparison, it can be observed that all the three samples have different anatomy in the rest configuration that would impact the overall surgical outcome for type 1 thyroplasty using the implants. Usage of PhonoSim on these subject specific samples would enable better surgical planning due to prior information on the anatomy thereby increasing the chances of obtaining favorable surgical outcome and reducing the chances of revision needed later.

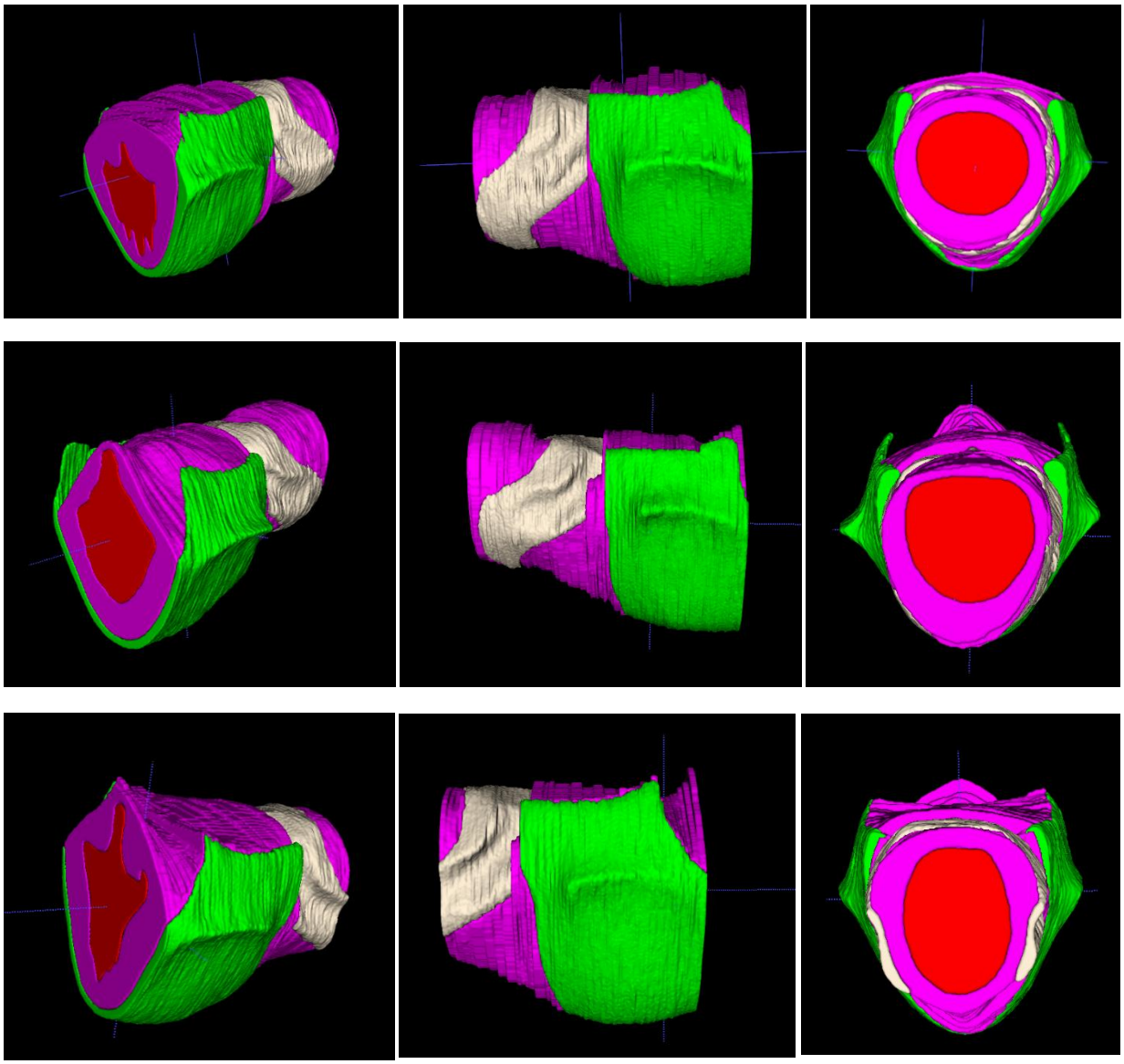

Figure 2.5: Manual Segmentation for sample 20, 21, 22 at configuration 0.

2.4.2 Configuration 1

The one side suture or configuration 1 is the configuration wherein one side of the rabbit larynx is subjected to the suture procedure which is the currently used practice for treating UVFP. Figure 2.6 shows the comparison between the three samples for configuration 1. Sample 20 corresponds to the first row, sample 21 corresponds to second row, and sample 22 corresponds to third row.

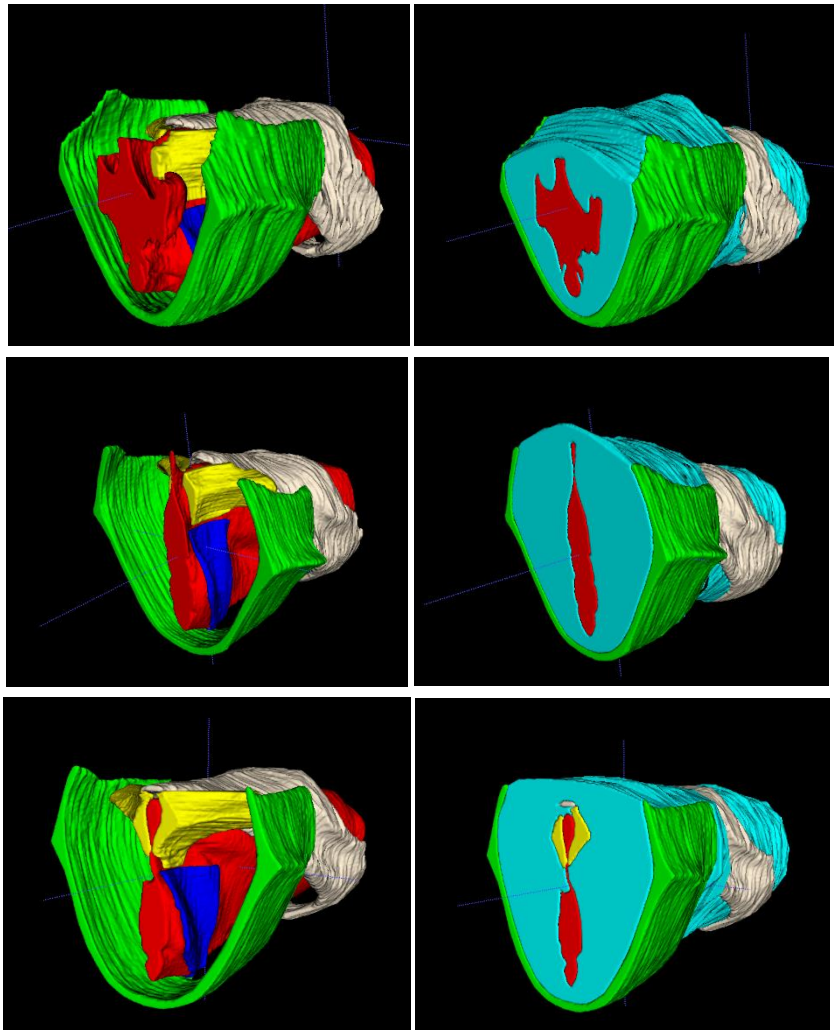

Figure 2.6: Manual Segmentation for Segmentation for sample 20, 21, 22 at configuration 1.

In this case, the difference in the surgical outcomes varies greatly between all the three samples. Due to the presence of a larger flow path for sample 20, it seems to have deformed the least in comparison to sample 21 and sample 22. For sample 21, the flowpath gets constricted and it reduces considerably near the entrance of the arytenoid cartilage. This would be problematic as it would not allow a problem interaction of arytenoid cartilage with the inspired and exhaled air impacting its performance and overall functioning. For sample 22, the deformation due to the surgery seems to be much more pronounced as a complete closure of airway is observed just below the arytenoid cartilage and above the vocal fold cover. A surgical revision would be needed in this situation as the patient would suffer difficulty in breathing due to this constriction in the airway. Other possible problems would include pulsating voice.

2.4.3 Configuration 2

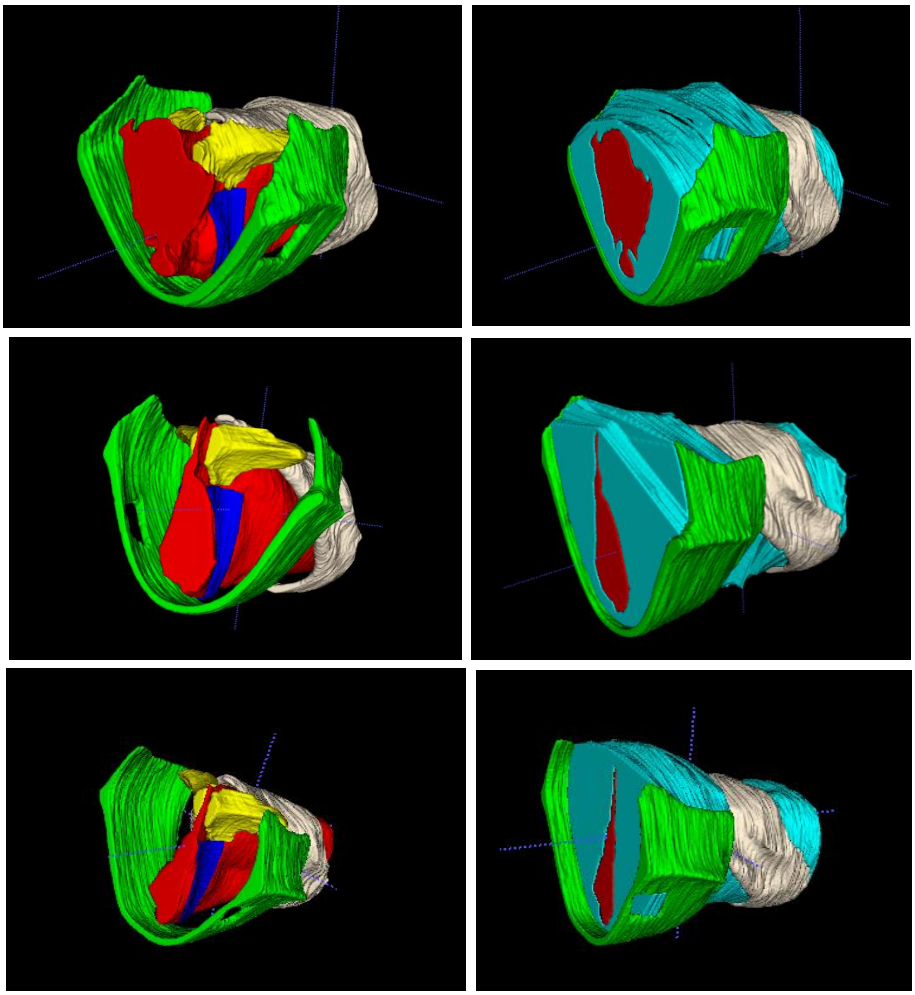

Figure 2.7: Manual Segmentation for sample 20, 21, 22 at configuration 2.

Figure 2.7 shows the comparison of the various samples under implant condition. The main difference in this segmentation stems from the presence of a window on the thyroid cartilage from which the implant insertion is made and pushed towards the vocal fold cover to correct the vocal fold position and hence alleviate the pain which the patient suffers from the UVFP. This is evident for the results of sample 21 and 22 in comparison with configuration 1. There is no constriction observed in both of these samples near the arytenoid cartilage which would ensure that the patient would have no difficulty in breathing. Analysis carried out by Li et. al. based on these samples also suggested that model guided implant surgery through PhonoSim for configuration 2 lead to better surgical outcomes[30].

2.5 Automation using the ITK-SNAP Tool

The ITK-SNAP Snake Tool, an implementation of Active Contour Segmentation, is a robust technique employed in medical image processing to precisely delineate and segment structures within images. This tool is based on machine learning to automatically segment the images after training with provided segmentation. Its salient features include user-defined initialization and customizable parameters, facilitating dynamic contour evaluation for real-time visualization and interactive refinement . In this study, we explored the usage of this tool to accelerate the segmentation process and create more robust segmentations. We provided the manual segmentations of Samples 21 and 22 as the training data and used Sample 20 as the test case.

Through the application of the ITK Snake tool segmentation, five distinct components of interest were successfully identified and subsequently segmented. These components encompassed the vocal fold cover, the thyroid cartilage, the lumen surface, the arytenoid cartilage, and the cricoid cartilage.

The segmentation process involved employing four types of pre-segmentation methods: Thresholding, Classification, Clustering, and Edge Attraction. As evidenced from the figures, it can be seen that this technique did well in identifying the surfaces but still requires additional fine tuning to give the final result as those surfaces were still coarse and blur out towards the edges where one or more components came in contact with each other. The limitation in this approach stemmed from the fact that most of the techniques use machine learning and require information such as predefined labels to function well. Owing to the limitations in the size of the training dataset, we couldn't explore the full use of neural networks to perform the segmentation tasks extensively. Usage of neural networks for medical image segmentation has been previously explored in the literature[34] and have shown promising results but tend to be very data hungry when it comes to training the model. Their use to automate the segmentation process would be explored in the future as they offer significant improvements in terms of saving time and dealing with complex geometries.

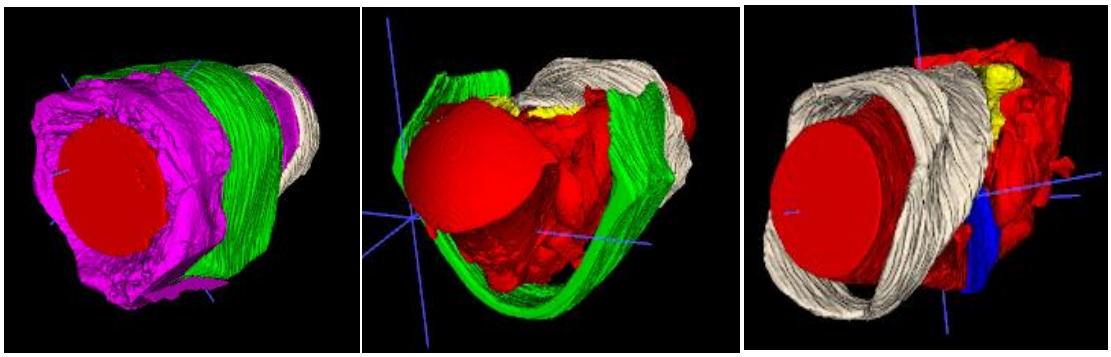

Figure 2.8: Snake tool implementation for sample 20 configuration 0, 1, and 2 (ordered left to right).

Figure 2.8 above shows the results obtained through the usage of snake tool for the sample 20 configurations

0,1, and 2. The labels used in the Snake Tool implementation are the similar to the ones used in manual segmentation with the only notable difference in color of the label for vocal muscle connecting all the components which is purple instead of light blue. The implementation was carried out only for sample 20 owing to time limitations. Figure 2.8 shows the individual components that are correctly segmented from the MRI scans, and their geometries are close to those obtained by the manual segmentations. The major issues encountered while using the Snake tool in this work stems from its inability to correct identify the boundaries between the segmented components. For instance, in the case of configuration 0, the shape of the vocal muscle connecting the various components is not smooth and would later require manual correction. For configuration 1 and configuration 2, the flow path shape was not as precise as compared to the manual segmentation results as it was unable to identify the exterior boundary where the flow path ends, and other components begin. In general, our results prove that this approach can be explored further. Better results could be obtained with a larger dataset to train the model on.

2.6 Results and Discussions

The results obtained from segmentation as described in this chapter can be used for subject-specific modeling to treat UVFP using type 1 thyroplasty, which can be demonstrated through the recent works carried out in our research group[7,28–30] . This work is a part of a greater research project in which our group aims to use a computational modeling-based tool, which we call PhonoSim, to provide pre-surgery guidance to surgeons to obtain better surgical outcomes. The segmented geometrical models obtained here will later be turned into FEM models which will then be imported into the in-house fluid-structure interaction (FSI) code to simulate the flow-induced vocal fold vibrations and determine the optimal location and design of the implant. Our group is currently performing comparative studies by comparing the impacts of ex-vivo and in-vivo surgeries with and without model guidance[7,28–30] . Recent work by Li et. al. shows the segmented samples 20 to 22 presented in this work have been utilized to perform a study on optimized implant placement, quantitative assessment of vocal fold adduction and implant placement error[30] . Their work showed that PhonoSim-guided implantation achieved higher vocal fold medialization relative to the controls. Another work by Li.et.al talks about using the segmented models to compute the eigen frequencies and eigenmodes for optimized implant placement[7] . Avhad et. al. have also shown the importance of having a robust segmentation protocol for achieving subject-specific models which can be used to simulate the vocal fold medialization and then the fluid-structure interaction of vocal folds[28,29] . Therefore, the segmentation described here is essential for the success of our overall PhonoSim project.

The major advantage of using the existing manual segmentation method is its ability to allow careful identification of subject-specific components related to the vocal fold physiological functions and thus provide accurate anatomical information that could be incorporated in the FEM model for subject-specific

simulations. The mesh generation process following our segmentation is a straightforward process, which allows the segmented model to be easily converted into FEM models using COMSOL. Another advantage is the usage of the freely available ITK-SNAP tool. This tool can handle a variety of medical imaging data like MRI and CT, it has a friendly graphical user interface (GUI) that allows each component to be labeled separately for easy identification. Both COMSOL and ITK-SNAP are extensively used in the research community and have a great community forum for discussion and quick solutions to any problem that is encountered while working on the project.

One major disadvantage of the manual method is that the overall segmentation process is time consuming and as a result, only a few samples could be segmented and used for subsequent FEM and FSI modeling in this project. In addition, sufficient knowledge of the vocal fold anatomy and substantial experiences of segmentation are required for successful completion of these tasks. For many samples and a large dataset, the current manual approach becomes impractical, and thus either semi-automated or fully automated approaches should be sought. Our usage of the snake tool in ITK-SNAP presents one of the ways to automate this process. For this project, we merely explored the usage of this tool and its feasibility. The results we obtained are promising. However, it is still not perfect as it suffers from the lack of enough input data to be trained on. Other neural network-based methods are possible for our application, but again they would require a bigger dataset size to be trained on. In addition to incorporate more datasets for training, future works may also involve exploring ITK programming package present in ITK-SNAP to automatically identify the required thresholds parameters for the clustering or classification algorithm that could be used for identifying the various anatomical components from a single imaging dataset.

CHAPTER 3

Segmentation and Computational Modeling of the ACS in Treating Obstructive Sleep Apnea

This chapter describes the development of the Obstructive Sleep Apnea (OSP) model from the medical imaging data and then using this FEM model to capture the effects of Ansa Cervicalis Stimulation (ACS) to treat the OSA. To achieve ACS condition, hook wire percutaneous electrodes were used to stimulate the right branch of the ansa cervicalis innervating the sternothyroid muscle during propofol sedation[22]. Kent et al. demonstrated that the stimulation of the ansa cervicalis branch targeting the sternothyroid muscle resulted in a notable increase in inspiratory airflow among obstructive sleep apnea (OSA) patients undergoing drug-induced sleep endoscopy (DISE)[22]. This intervention independently augmented airflow response during flow-limited hypopharyngeal negative pressure system (HNS), indicating enhanced upper airway patency. These findings collectively suggest that ansa cervicalis stimulation (ACS) effectively stabilized pharyngeal patency in OSA patients, potentially offering additional benefits to those with incomplete responses to HNS. The pharyngeal stabilization induced by ACS is attributed to the caudal traction exerted by the sternothyroid muscle, which acts by pulling the thyroid cartilage downward, akin to the tracheal traction observed in prior animal and human investigations. Animal studies have shown that caudal traction reduces peripharyngeal tissue pressure, enhances pharyngeal wall compliance, and increases tension along the distal edge of the soft palate, consequently improving upper airway patency[35] . Similarly, in humans, tracheal traction has been associated with decreased collapsibility of the pharynx, leading to reduced airflow obstruction during sleep[36].

Recent research by Kent et al. underscores that caudal traction from sternothyroid muscle contraction yields substantial enhancements in airway patency, further supporting the efficacy of ACS in managing OSA-related airflow limitations[22]. They also observed further improvements in pharyngeal patency when ACS was superimposed on HNS, suggesting different mechanisms for stabilizing pharyngeal patency. Rowley et al.[37] observed synergistic interactions between tongue protrusion and tracheal traction concerning pharyngeal collapsibility in an isolated feline upper airway model. Their findings revealed that the combined effect of these interventions surpassed that of each intervention individually. The researchers hypothesized that tracheal traction led to a reduction in pharyngeal wall compliance by increasing longitudinal tension. Conversely, tongue displacement primarily exerted outward dilating forces on the pharynx. The concurrent manipulation of both mechanisms resulted in the most significant overall alterations in pharyngeal collapsibility, as the effects of tongue displacement were magnified when applied alongside tracheal traction, particularly evident in stiffened pharyngeal walls. Kent et. al. findings showed a similar synergistic effect when HNS and ACS were combined[22]. The stimulation specifically targeted the sternothyroid muscle in their

study. This choice was made based on several factors. Firstly, this muscle is recognized for its capacity to apply caudal traction on the pharynx, a feature observed in both rabbits and humans, wherein both species possess a freely suspended and mobile hyolaryngeal complex. Additionally, in rabbits, investigations have revealed that the sternothyroid muscle exhibits a considerable mechanical advantage over the sternohyoid muscle. Second, the innervation of the sternothyroid muscle is readily accessible and anatomically reliable.

Although ACS has been shown a promising approach to treat the OSA, its biomechanical mechanisms are still not clear. As a result, its effectiveness on individual patients is also not clear. To fill the knowledge gap, we aim to develop an FEM model for the OSA and ACS to study the deformation of the tissues involved in this treatment process. Such FEM models will help understand from the physical principles how the ACS works for the OSA and in addition, it could be potentially being used to predict the effectiveness of individual OSA patients who are considered for the ACS procedure.

3.1 Segmentation and Mesh Generation

The overall procedure of model construction is provided here. A CT scan of an OSA patient was used to segment the various components related to the OSA and ACS. After completing the segmentation, an FEM model is generated for the entire body using AutoDesk Meshmixer and COSMOL Multiphysics. This process was repeated for the individual components and these individual segmented components were flagged on the unified airway model referred as the unified mesh. This model was then imported into COMSOL and each flagged component on the unified mesh was assigned with the proper material properties. The FEM model will be used to simulate the tissue deformation with or without the ACS, and the two cases will be compared to study effect of the ACS on the tissue displacement. The process of segmentation and mesh generation for the OSA sample is similar to that for UVFP. In the case of the OSA patient, the image dataset was a CT scan obtained from the NIH patient database provided by Dr. Yike Li. The image was segmented in ITK-SNAP and then exported to the Mesh Mixer and then smoothened to remove the uneven surfaces. For developing the computational model, the following components were identified during segmentation: jawbone, pharynx wall, tongue, epiglottis, cricoid cartilage, vocal fold soft tissue, hyoid bone, thyroid cartilage, soft palate, hypothyroid muscles, and the connective soft tissue between jawbone and the pharynx wall . The mesh was then exported to COMSOL to generate an unstructured mesh consisting of tetrahedral volume elements and triangular surface elements. The following points describe the process in detail:

i. Identify and segment the individual components related to the OSA and ACS. Figure 3.1 shows the segmentation procedure in ITK-SNAP, where individual components were colored and identified. Segmentation was carried out along the axial, coronal, and sagittal directions.

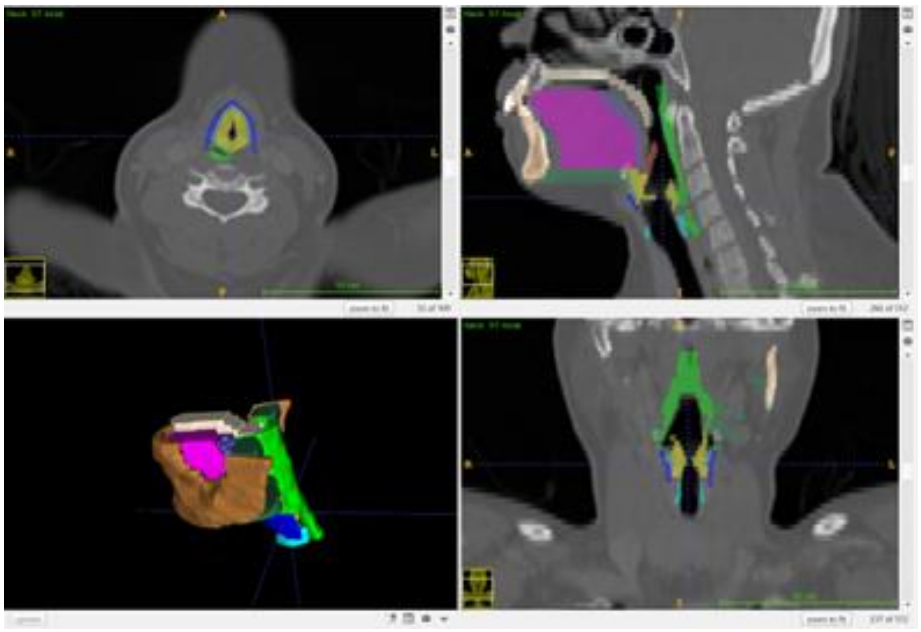

Figure 3.1: ITK-SNAP window in the segmentation process for an OSA patient.

ii. Surfaces of the segmented components were then exported from ITK-SNAP as shown in Figure 3.2.

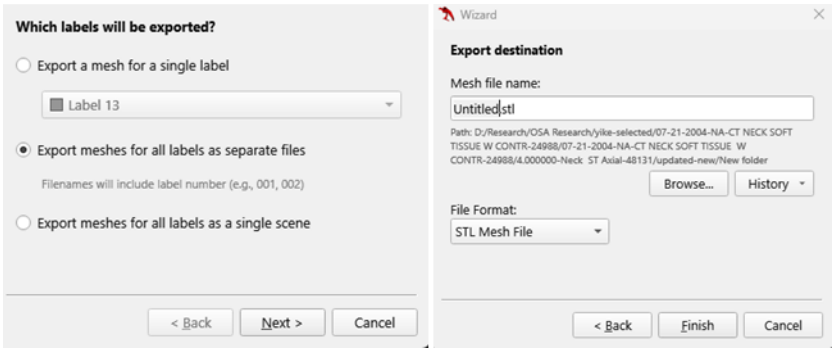

Figure 3.2: Exporting the surface mesh from ITK-SNAP.

iii. After exporting the surface mesh for all the components, each component was exported individually into Mesh Mixer and then smoothened out to remove the uneven surfaces. Figures 3.3 and 3.4 show this process.

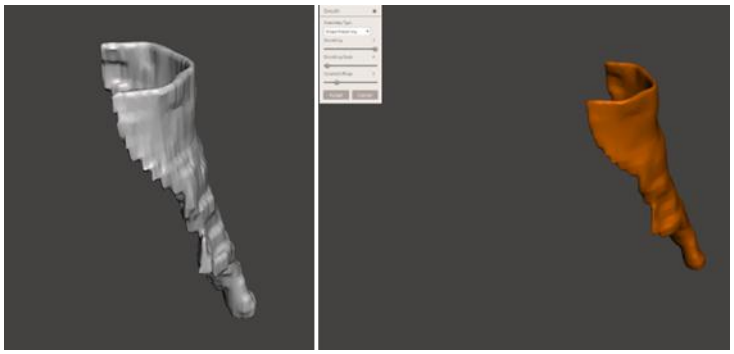

Figure 3.3: Smoothening process in Mesh Mixer to remove the uneven surfaces of individual components. Left: before smoothing; right: after smoothing.

Once the component is smoothened out, the component is remeshed. This smoothened-out component is then exported to COMSOL.

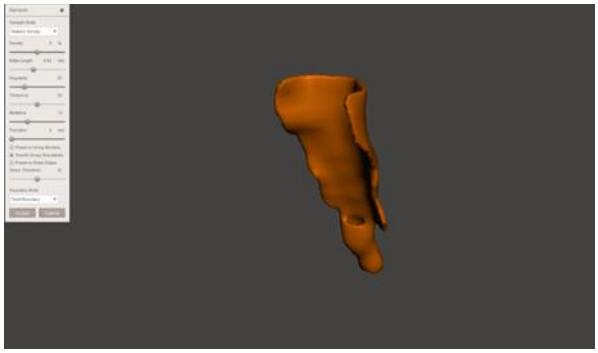

Figure 3.4: Remeshed component ready to be exported to COMSOL.

iv. The smoothened-out component was then imported into COMSOL, and a mesh was generated for this individual component. Figure 3.5 below shows the generated COMSOL mesh for the pharynx.

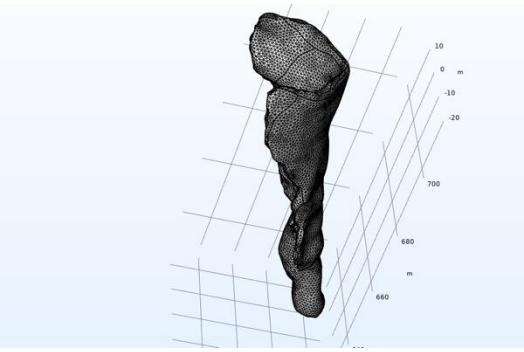

Figure 3.5: Final generated mesh with individual components identified.

v. Once the mesh was generated, it was exported as a Nastran (.nas file) for performing further modifications. The format for exporting the mesh was to select “Free” and “export it as linear elements” under the export options. The exported mesh was written as a Nastran file in the destination folder.

vi. The process was repeated for all the components as well as for the unified mesh which consisted of all the components mapped under a single surface mesh or label.

3.2 Image Segmentation Results

The segmentation process, the essential components generated were the cricoid cartilage, jawbone, thyroid cartilage, tongue, soft palate (together with hard palate), pharynx wall, epiglottis, hyoid bone, hypothyroid muscle, vocal fold tissue, and the other soft tissues. Figure 3.6 and Figure 3.7 represent the meshmixer smoothened-out images of these components as well as the unified body.

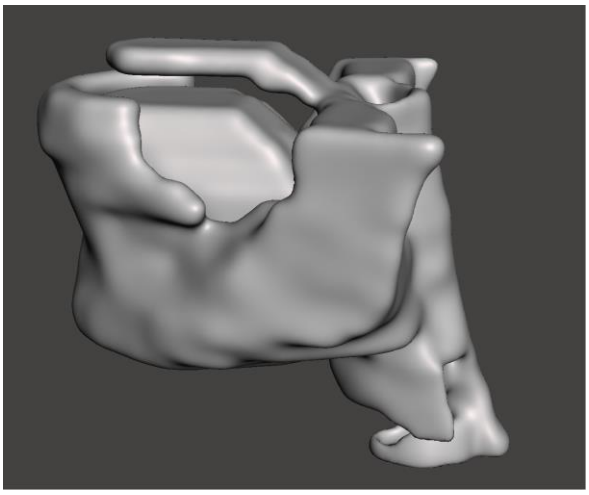

Figure 3.6: The unified body mesh.

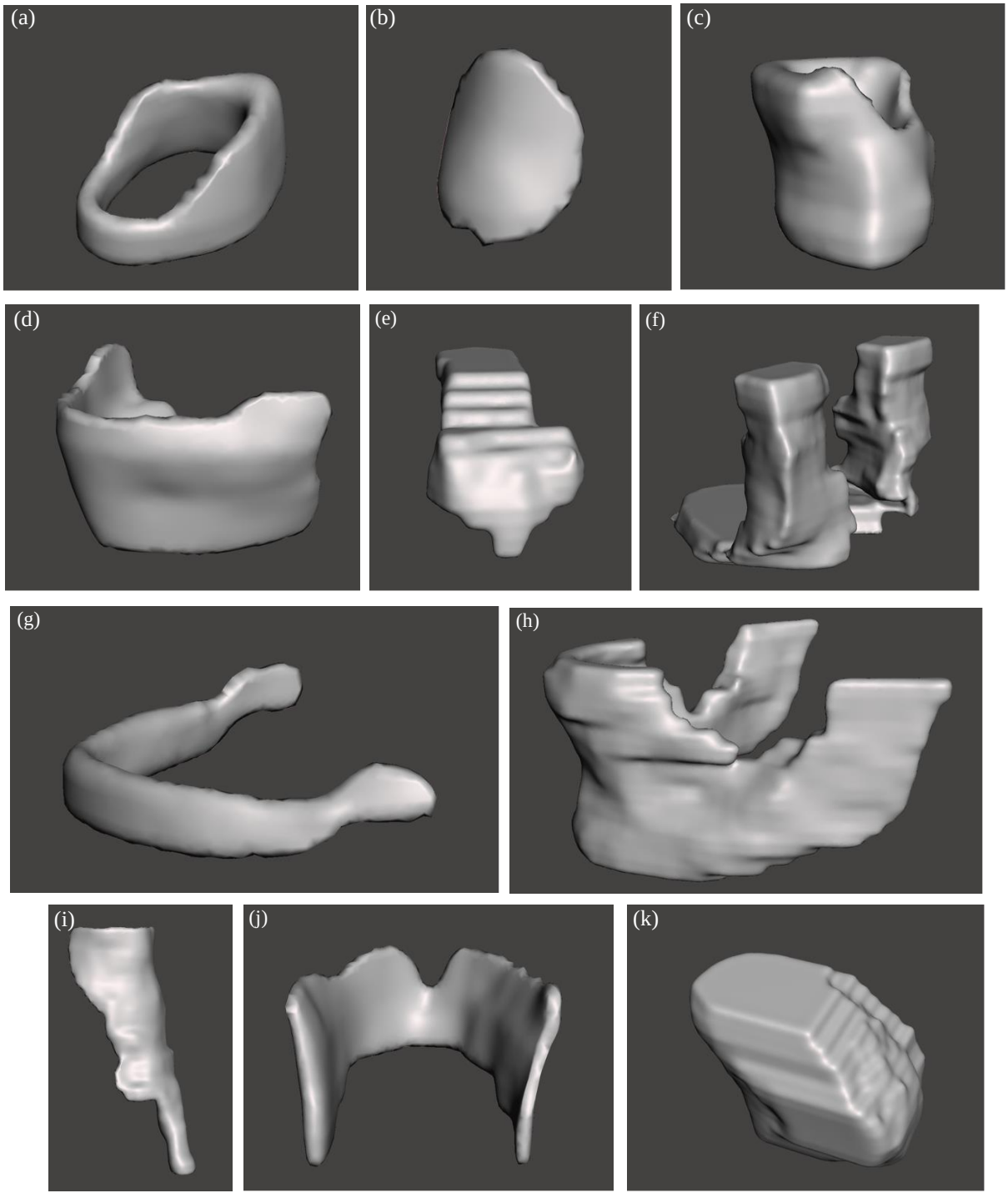

Figure 3.7: Smoothened out components. (a)=cricoid cartilage, (b)= epiglottis, (c)= The soft vocal fold tissue, (d)= Thyrohyoid muscle, (e)= The soft palate (which includes the hard palate that will be fixed), (f)= The soft oral tissue, (g)= The hyoid bone, (h)= The jawbone, (i)=The pharynx wall, (j)= The thyroid cartilage, (k)=The tongue.

3.3 Flagging the Individual Components on the Unified Mesh

After obtaining the Nastran files of individual components as well as the unified mesh on which the individual components have not been identified, a MATLAB script read in all these mesh data from multiple files and went through a registration process, in which the individual components were identified or flagged on the unified mesh by comparing the individual mesh and with the unified mesh. The script follows the algorithm below:

i. **Importing Mesh Data:** Initially, the script reads mesh data from multiple input files, including a unified body mesh and the separate files for various anatomical components like the pharynx, epiglottis, soft palate, cartilages, and the soft tissue components.

ii. **Mesh Manipulation:** The script then processes the body mesh data by adding edge nodes to the mesh and updating the element connectivity to maintain mesh integrity while increasing resolution.

iii. **Distance Calculation:** For each node on the body mesh, the script calculates its distances to all the nodes on an anatomical component. The shortest distance is then found and is defined as the distance of this body mesh node to the individual anatomical component.

iv. **Node Flagging:** After the distances to all the individual components are calculated, then these distances are compared, and then the shortest one is found. The corresponding component is then deemed to be represented by this node on the body mesh. That is, this body mesh node is flagged as the corresponding component. By repeating this procedure for all the nodes on the body mesh, then every node is flagged as an individual component according to its nearest anatomical component. As the result, all individual components are on the same mesh without any gap or mismatch of mesh nodes.

v. **Element Flagging:** Similarly, all the tetrahedral elements on the body mesh are flagged as individual components based on its vertex flags. The most representative flag of the vertices is used for the element flag. This allows for later assignment of the tissue properties for the individual elements according to its component identity.

vi. **Output Generation:** Finally, the script generates an output file containing the unified body mesh with flagged nodes and elements.

Figure 3.8 shows the visualization of the output obtained from the algorithm in Paraview. Each component that is flagged can be identified by a different color. Since a total of 11 components were segmented, 11 flags were generated by the MATLAB script correspondingly.

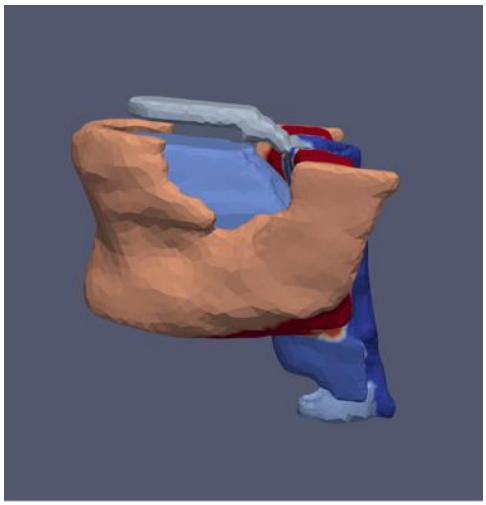

Figure 3.8: Individually flagged components on the unified mesh.

Figure 3.9 shows the final COMSOL mesh with the flagged components that were generated using the script. This model would be utilized for conducting the biomechanics simulation in COMSOL.

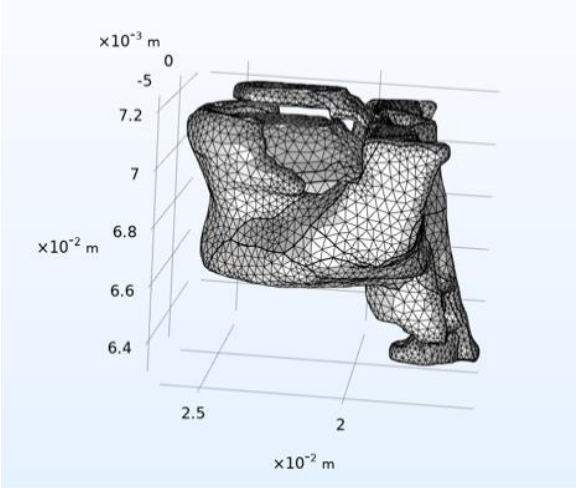

Figure 3.9: Final Generated Mesh with flagged components.

3.4 Setting up the Tissue Biomechanics Model in COMSOL

To set up the biomechanics study in COMSOL, the Solid Mechanics module was selected, and a stationary study was performed. The flagged individual components on the unified mesh were assigned corresponding material properties as specified in Table 1. All components are assumed to be linear elastic in this study, but

nonlinear strains were enabled to handle potential large displacements and large rotations. This is because determining the material properties of the individual components proved to be challenging due to the lack of uniformity in the literature. For most of the components there was a huge variation in material properties from the values in the ranges of kPa to MPa in some cases[38–42]. To simplify the study and develop a proof-of-concept model that could be used to support the results obtained by the Ansa cervicalis stimulation experimentally, the use of linear materials was determined to be the best way here. Depending on the results, nonlinear properties could be added to the components, if necessary, e.g., the tongue, which is known to have a very complex structure and experience large deformations.

SI. No	**Component**	**Density (kg/m^3)**	**Youngs Modulus (Pa)**	**Poisson's Ratio**	**Reference**
1.	Jawbone	1090	1000000	0.22	Wang et. al.[42]
2.	Pharynx wall	960	5000	0.35	Burd et. al.[41]
3.	Tongue	1040	30000	0.499	Cheng et. al. [39]
4.	Epiglottis	1040	25000	0.49	Burd et. al.[41]
5.	Cricoid	1100	100000	0.49	Gagnon et. al.[43]
6.	Vocal Tissue	1090	100000	0.32	Gagnon et. al.[43]
7.	Hyoid bone	1908	100000	0.32	Min et. al.[44]
8.	Thyroid	1100	100000	0.49	Gagnon et. al.[43]
9.	Soft Palate	1040	15000	0.32	Luo et. al.[45]
10.	Oral tissue	1090	5000	0.49	Carrigy et. al.[46]
11.	Thyrohyoid muscle	1090	15000	0.35	Hermant et. al.[47]

Table 3.1: Material properties used for the different components for the solid mechanics simulation of OSA.

After specifying the material properties, boundary conditions needed to be applied for various surfaces. These boundary conditions are as follows:

i. Fixed constraints: The hard palate and jawbone were assumed to be a fixed constraint as highlighted by blue color in the figure below. The hard palate is a stiff component that doesn't deform much in the experiment and was thus simply assumed to be fixed. The jawbone is also a stiff structure with very high Young's modulus, and in addition, it was assumed to be stationary in the process.

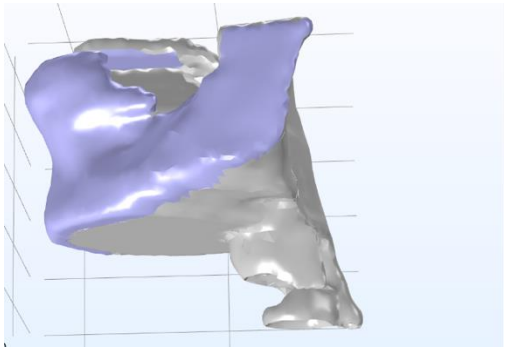

Figure 3.10: Fixed constraint applied to the COMSOL model.

ii. Boundary Load: A stimulation load of 1N in the z-direction that mimics the Ansa cervicalis stimulation was applied to the model to enable the biomechanics simulation as shown below in figure 3.11. During the stimulation, the sternothyroid muscle contracted, which pulls the thyroid cartilage down toward the collar bone. Therefore, we applied the load on the thyroid cartilage near its bottom anterior since the sternothyroid muscle is anchored on the anterior side of the thyroid cartilage. The load would cause the cartilage to move down as well tilt forward.

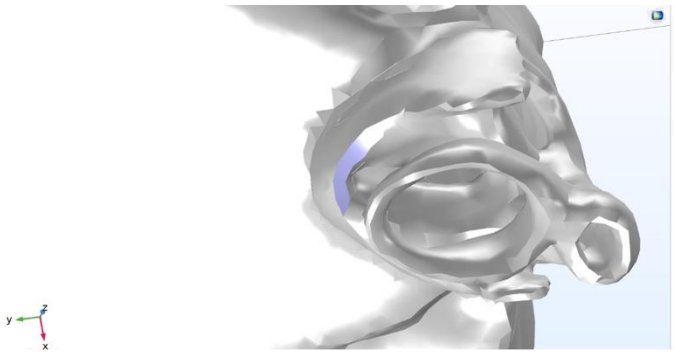

Figure 3.11: Stimulation load applied to the thyroid cartilage.

iii. Prescribed Displacement: The cricoid was constrained to move only in the z-direction, and its motion was constraint along the x- and y-directions. This was done to ensure that the unnatural horizontal translation and rotation of the cricoid cartilage were avoided. Figure 3.12 below shows this.

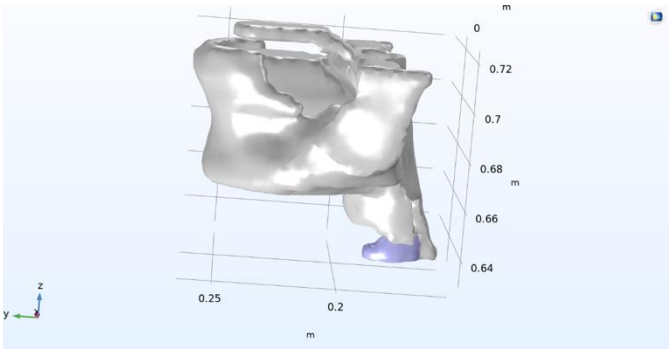

Figure 3.12: Prescribed displacement for the cricoid cartilage.

iv. Pharynx Wall Displacement: The top side of the pharynx wall was fixed as shown in figure 3.13. This is because the nasal cavity which is located above the pharynx wall was assumed to have limited movement during OSA or stimulation, and thus the top of the pharynx could be assume a fixed constraint, but the rest of its body may move.

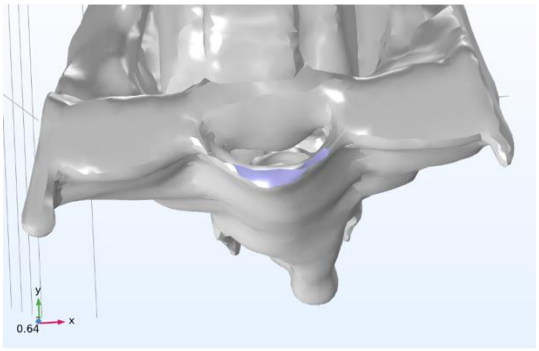

Figure 3.13: The top of the pharynx wall was fixed.

v. The pharynx wall movement: The pharynx wall was constrained to “slide” down only because of its attachment to the spine. To incorporate the natural slope of the wall in the yz-plane, the y-displacement and the z-displacement were constrained so that w=0.8*v, where w represents the displacement in the z-direction and v represents the displacement along the y-direction. The factor of 0.8 was chosen as it represents the slope of the pharynx wall.

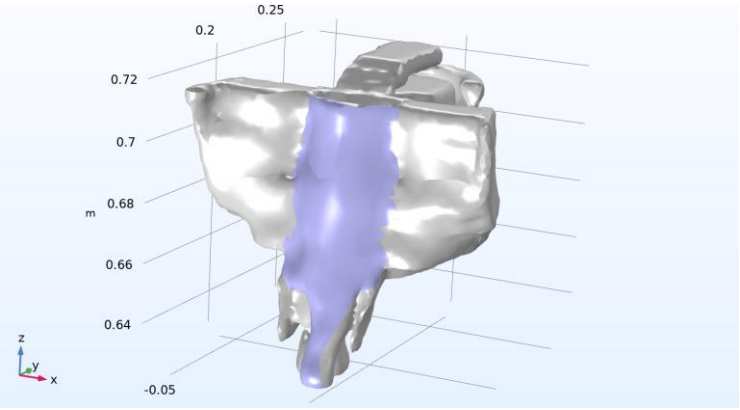

Figure 3.14: The constraint on the pharynx wall movement.

vi. Gravity Load: In the study, we considered the effect of the gravity load. In that case, the tongue was subjected to a gravity load in the posterior direction to represent the supine position, where the tongue base may move toward the pharynx wall and close the airway. Gravity was modeled as a volumetric load on the tongue. This is shown by figure 3.15. A gravity load of *g* was applied to the tongue in the negative y direction.

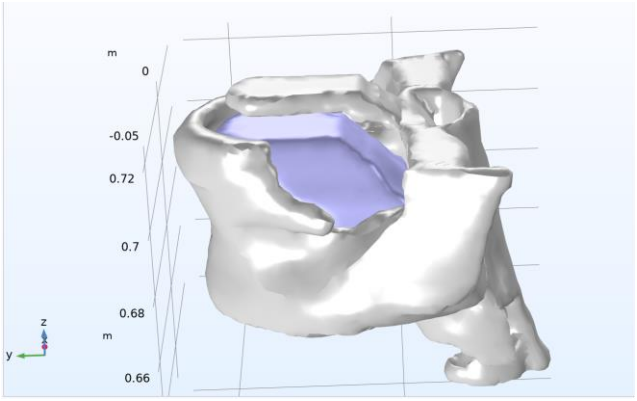

Figure 3.15: Gravity Load on tongue.

vii. Pressure Load: A In addition to the gravity load on the tongue, we also considered the negative pressure load that is incurred when breathing, which may cause collapse of airway in OSA. Here we applied the negative pressure load to the posterior tongue surface, the posterior surface of the epiglottis, and the interior surface of the pharynx wall since these structures are subject to the negative pressure and may be prone to collapse. This load is observed in the figure below. A negative pressure of -50 Pa was

applied in this study.

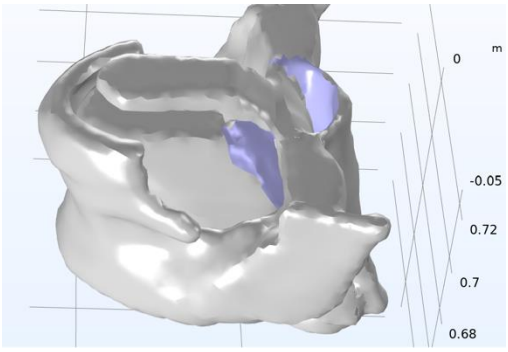

Figure 3.16: A negative pressure load applied to the tongue, epiglottis, pharynx wall, and soft palate.

3.5 Simulation Results

For the COMSOL simulation, three different situations were studied to understand the effects of ansa cervicalis stimulation and how it helps obtain desired outcomes when treating OSA. These three situations are: 1) with and without stimulation in the absence of other loads, 2) with and without stimulation in the presence of gravity load, 3) with and without stimulation in the presence of the negative pressure load. In each situation, we will study the effect of stimulation on alleviation of the OSA.

3.5.1 Effect of Stimulation in the Absence of Other Loads

The effect of stimulation stems from the application of the stimulation load specified in section 3.4 under a boundary load pulling down the thyroid cartilage. A stimulation load of 1 N is applied in the negative z-direction. By comparing Figure 3.17 and Figure 3.18, it can be seen that the stimulation load causes the tongue to tilt toward the posterior direction.

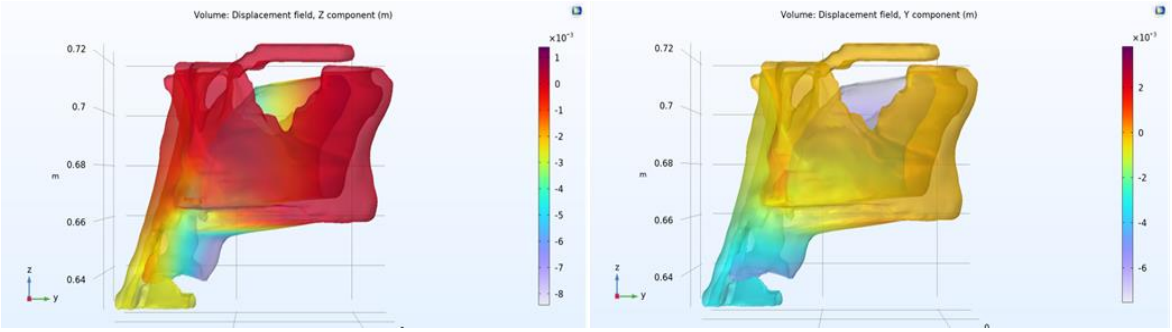

Figure 3.17: Effect of stimulation load

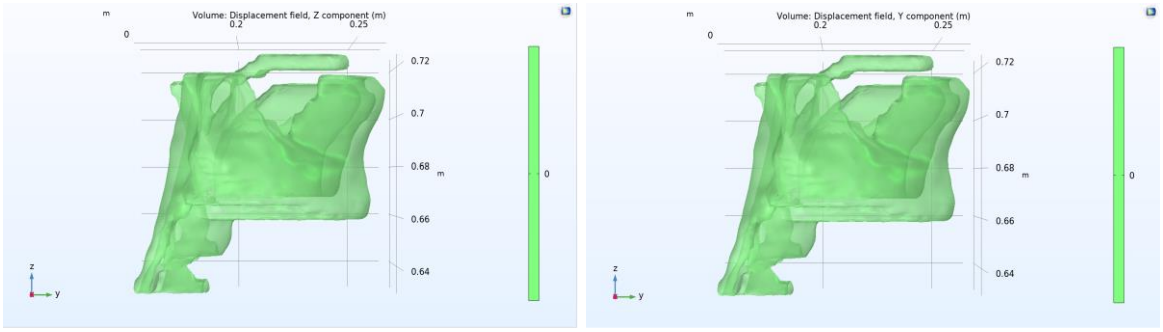

Figure 3.18: The model without the stimulation load applied.

To better see the displacements of the interior structures such as epiglottis and the soft palate, a 2D slice along the vertical midplane was taken which helps in understanding the effects of the stimulation load on those components.

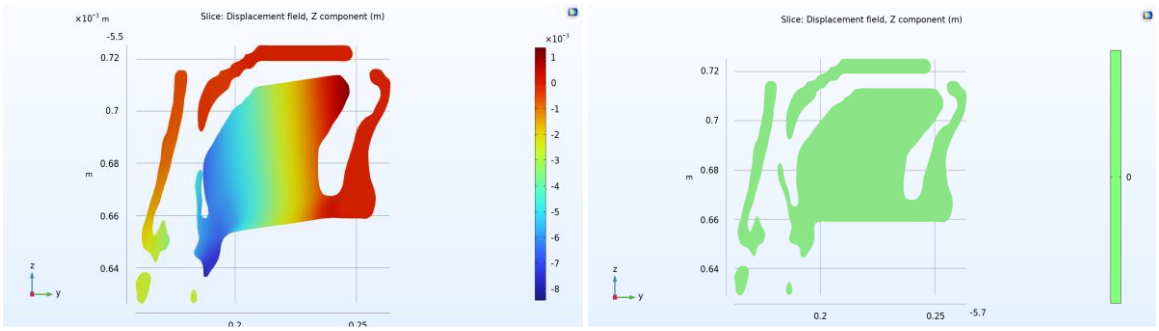

Figure 3.19: z-direction displacement slice for stimulation (left) and no stimulation (right).

Figure 3.19 and Figure 3.20 show the comparison of the stimulation load and non-stimulation load conditions along the z-direction and y-direction respectively using a slice along the midplane. From Figure 3.19 and Figure 3.20, it can be seen that in the left images where the effect of stimulation was captured, the epiglottis stands up and clearly moves away from the pharynx wall when compared to the images on the right where no stimulation load was applied. This deformation is caused since the base of the epiglottis has a curvature, and when the base is being displaced under load, the curvature becomes greater, which causes the tip of the epiglottis to move up and to the anterior. Another result to note is that the pharynx wall is stretched down due to the stimulation load. This effect may help stiffen the pharynx wall and prevent it from collapsing under the negative pressure load. The soft palate also deforms slightly by moving down, but its displacement is

only around 0.6 to 1 mm.

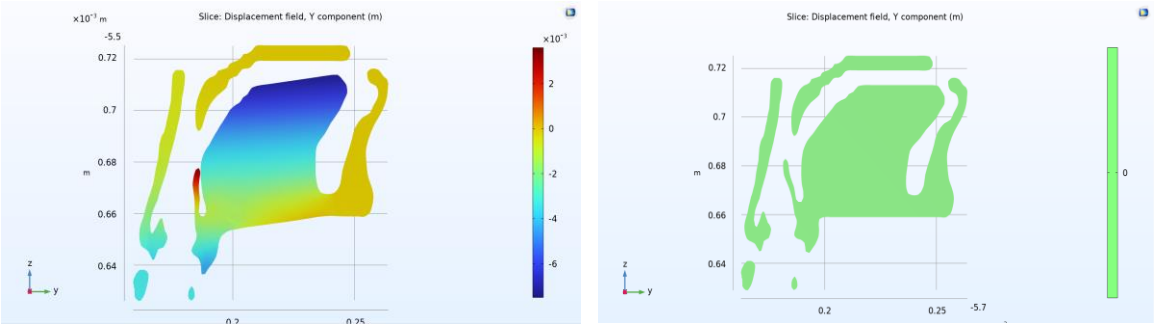

Figure 3.20: y-direction displacement slice for stimulation (left) and no stimulation (right).

3.5.2 Effect of Gravity Load with and without Stimulation

The OSA condition is typically encountered in patients with high body mass index (BMI) sleeping in supine position. In that position, the tongue moves under the influence of gravity and tends to close the airway by eventually hitting the pharynx wall. While this effect cannot be completely captured in this study owing to the specific geometry of the patient tongue, and also perhaps the linear material assumption for the tongue, we will still examine its displacement and discuss the possible alternative results. Figures 3.21 and 3.22 show the 3D structure from an external view without and with the stimulation load, respectively. The displacement of the thyroid cartilage is clear when the stimulation is applied. However, in both cases, the tongue tilts up toward the hard palate, and a comparison of the interior view is needed.

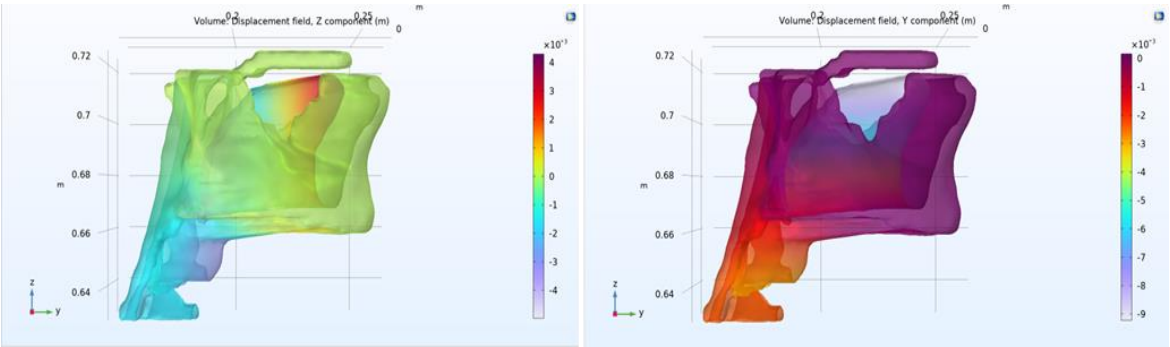

Figure 3.21: Effect of gravity load on the model without stimulation load.

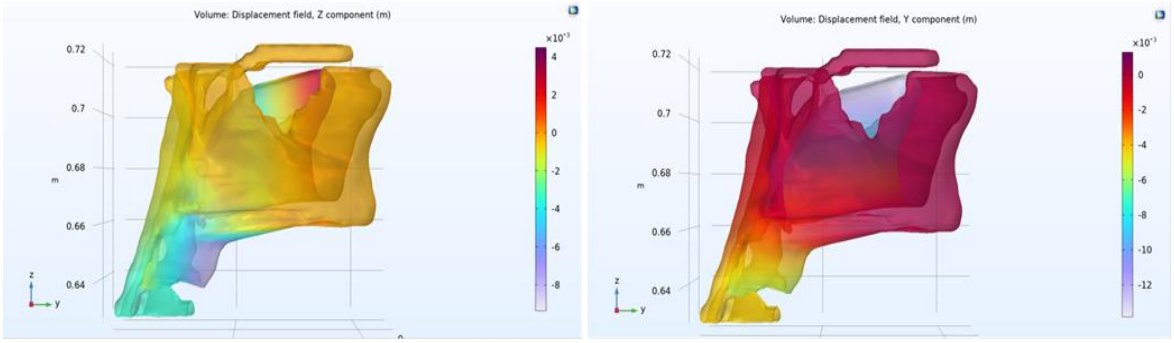

Figure 3.22: Effect of gravity load with the stimulation load.

Figures 3.23 and 3.24 show the z-displacement and y-displacement, respectively, along the 2D slice in the midplane. From these figures, it can be seen that although the tongue tilts up toward the hard palate in both cases (with and without gravity), the tongue base moves further down due to the stimulation. Because of the specific shape of the tongue base in this case, the tilting of the tongue causes the tongue surface to be a little closer to the pharynx wall. We believe for some shapes of tongue, the downward movement of the tongue base may cause the tongue surface to move away from the pharynx wall.

In the case of stimulation, the epiglottis again stands up and moves away from the pharynx wall. If contact is activated, the epiglottis may come in touch with the tongue base and help prevent it from collapsing.

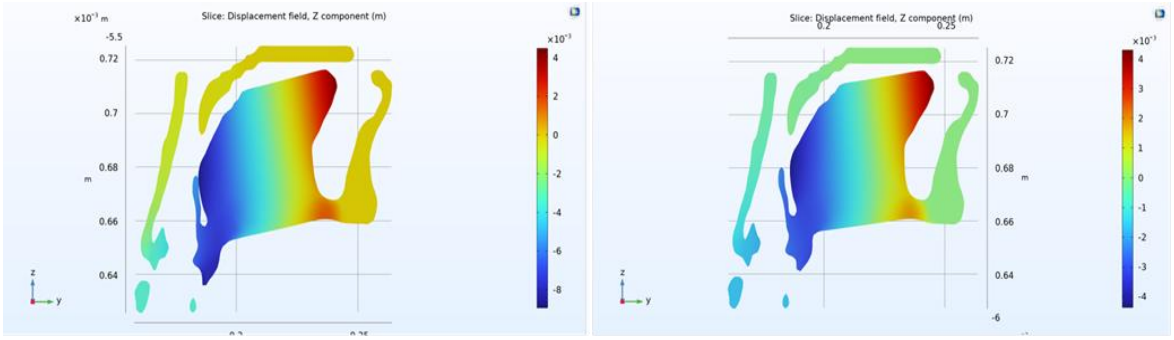

Figure 3.23: The z-displacement slice for gravity load with stimulation (left) and no stimulation (right).

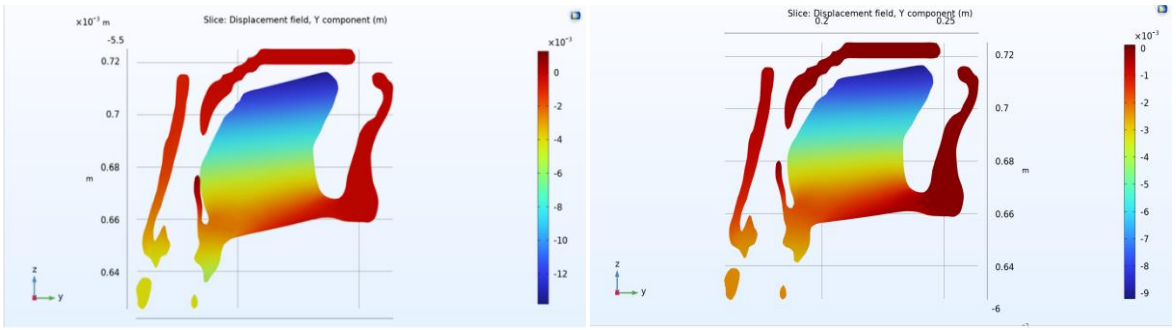

Figure 3.24 : The y-displacement slice for gravity load with stimulation (left) and no stimulation (right).

3.5.3 Effect of a Negative Pressure Load with and without Stimulation

Understanding the effect of the negative pressure in the oral cavity is important because the negative pressure in the airway caused by inspiration may cause the airway to contract, which in turn exacerbates the negative pressure and causes the airway to further collapse. In our study, a negative pressure load of -50 N is applied along the inner surface of the pharynx wall, the posterior soft palate, and the posterior tongue surface to model this situation as described in section 3.4. A separate negative pressure load of -10 N is applied on the posterior epiglottis surface.

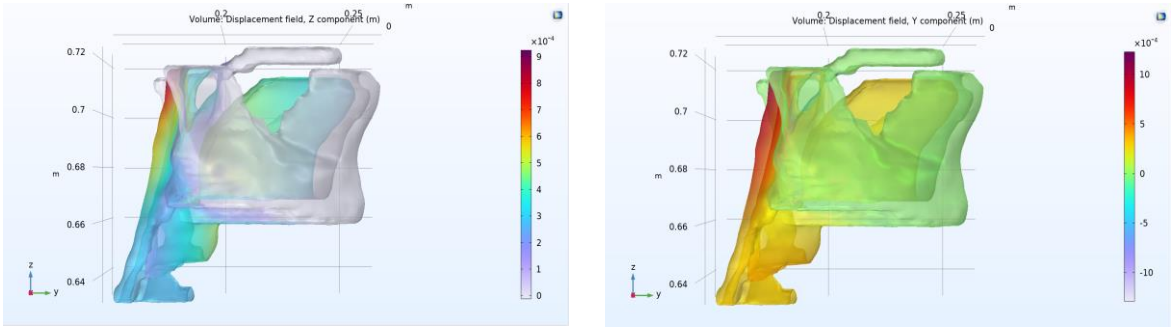

Figure 3.25: Effect of the negative pressure load on the model without stimulation load.

Figures 3.25 and 3.26 show the 3D model for the case of negative pressure load applied to the model without the stimulation, the negative pressure load causes the pharynx wall to be displaced towards the airway by 0.9 mm and also to stretch and stiffen from the external view of the 3D model.

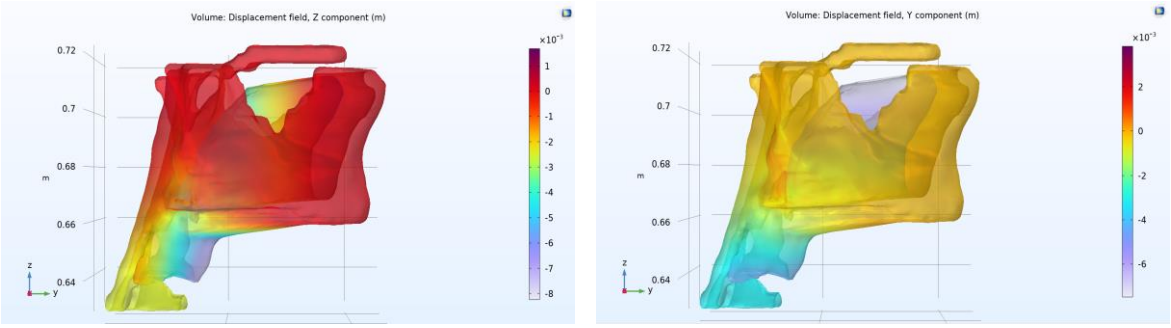

Figure 3.26: Effect of negative pressure load on the model with stimulation load.

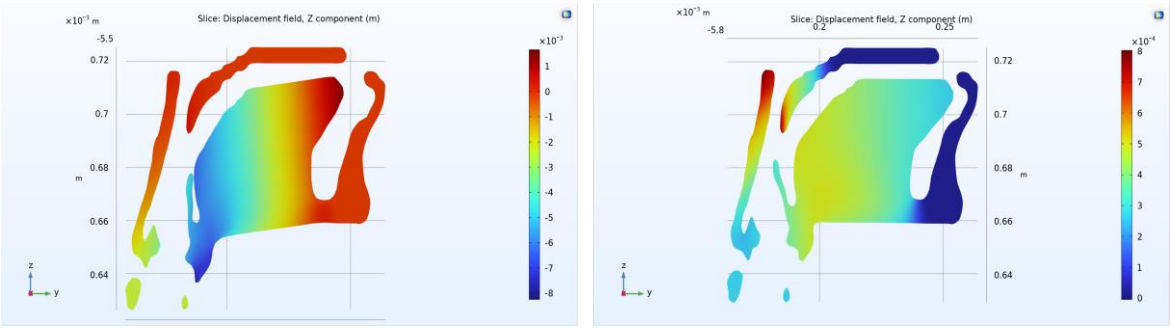

Figure 3.27: The z- displacement slice for negative pressure load with stimulation (left) and without stimulation (right).

Figures 3.27 and 3.28 show the 2D slice plots of the z- and y-displacements. Without the application of stimulation load, the soft palate deforms and moves towards the pharynx wall towards the tongue. The tongue deformation is negligible in comparison to the soft palate. It can be seen that even under the negative pressure load that tends to collapse the epiglottis, the stimulation still causes the epiglottis to stand up and move away from the pharynx wall. The epiglottis moves towards the tongue by 2 mm. The pharynx wall is still being stretched by the stimulation, which may generate a stiffening effect. From the y-displacement in Figure 3.28, under the negative pressure the soft palate tends to move toward the pharynx wall without stimulation. However, once the stimulation is activated, such unfavorable displacement becomes smaller. Therefore, the stimulation provides a beneficial effect on the soft palate deformation.

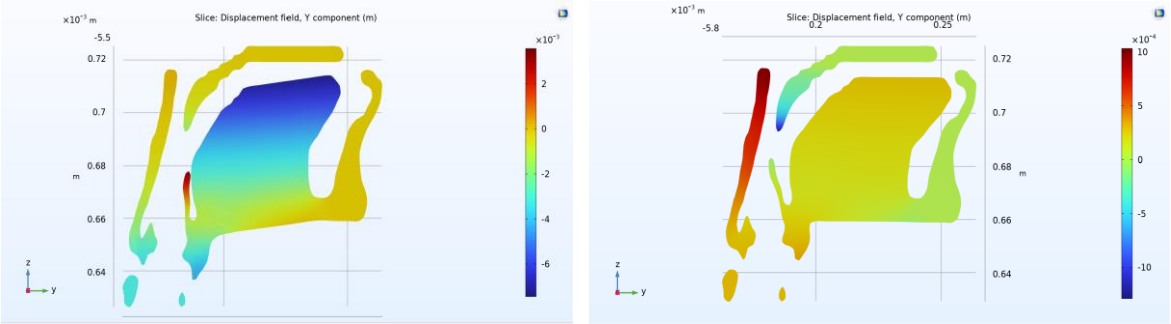

Figure 3.28: The y-direction displacement slice for negative pressure load with stimulation (left) and without stimulation (right)

3.6 Discussions

The current method used for segmentation and mesh generation of the human airway allows us to identify and capture patient-specific anatomical features in the airway reconstruction. The method is flexible in that we can easily add additional components, or remove certain components, through the manual segmentation and the automated registration (for individual components). This capability is useful in the present OSA study since we had to add additional components in the model several times based on the model results. The segmentation method allows us to easily modify based on previous segmentation results. The algorithm for flagging or labeling the individual components on the unified mesh ensures an integrated mesh on which different components can be correctly connected to each other without mesh mismatch. To our knowledge, the FEM model we have developed is the first attempt to model the effect of ansa cervicalis stimulation and study its biomechanical mechanisms in treating OSA.

Our computational model correctly captures the movement of thyroid cartilage being pulled caudally under the stimulation. As a result, the epiglottis stands up and moves away from the pharynx wall, causing the airway to open up and helping treat the OSA. The pharynx wall is also under extension by the stimulation and thus may become stiffened and less prone to collapse. All these effects have been observed by Kent et. al.[22,23] in their work which describes ansa cervicalis stimulation to provide caudal traction which improves pharyngeal patency by reducing its collapsibility, which reduces airflow obstruction during sleep. The models with the gravity and negative pressure loads showed consistent results in the movements of those key components. That is, the epiglottis moves away from the pharynx wall, the tongue tilts upward, and the pharynx wall extends downward. These results are qualitatively consistent with the experimental findings.

One major drawback of the model is that it didn't clearly show the benefit of the stimulation on the tongue movement away from the pharynx wall, which was observed in the experiment. The reason for this is most

likely because of the specific patient data we used, where the tongue didn't benefit much from the stimulation due to its geometry. In addition, the simple material properties that we used for the tongue also limit its deformation. Many studies in literature have modeled tongue to be a non-linear dynamic material[34,47,48].

Another limitation of this study is that we did not apply the contact between the individual surfaces, e.g., between the tongue and the soft palate. The experiments have shown that during the stimulation, the tongue moves down and its contact with the soft palate can be reduced under stimulation, which would be beneficial for opening of the soft palate. The tongue would also be expected to come in contact with the epiglottis when the gravity or negative pressure is applied. These effects were not modelled in this study.

CHAPTER 4

Conclusions and Future Work

Through this work, a robust computational modeling pipeline has been developed for developing subject-specific computational models using the CT and MRI imaging data for patients suffering from upper airway diseases such as the OSA and UVFP. Image segmentation was performed, and its results are presented for three New Zealand rabbit samples for the case of UVFP. Similar reconstruction was performed for one human sample from NIH database for the case of OSA. For the case of UVFP, the following components related to the physiological functions of the vocal fold were identified and segmented: thyroid cartilage, arytenoid cartilage, cricoid cartilage, vocal fold cover, and air path. For each of the sample, three configurations were segmented: the rest condition, one-side suture condition representing the UVFP, and one-side-suture-and-one-side-implant representing the type 1 thyroplasty. The segmented images show that these key components were capture in the reconstruction and thus they could be used for subsequent FEM and FSI modeling of the vocal fold. The use of the snake tool functionality in ITK-SNAP has also been explored to automate the image segmentation process which is currently carried out manually. The machine learning based tool shows promise in automating the segmentation process.

A proof-of-concept study for developing a computational model for treating OSA using ansa cervicalis stimulation was carried out in this study. The following components were identified and segmented: jawbone, pharynx wall, tongue, epiglottis, cricoid cartilage, vocal fold tissue, hyoid bone, thyroid cartilage, soft palate, oral tissue, and hypothyroid muscle. Extensive literature review was performed to determine the material properties for the identified components. These components were flagged on a unified body mesh, which was then exported into COMSOL for solid mechanics simulation. The applicable boundary conditions were identified and applied to model the conditions prevalent during the time of ansa cervicalis stimulation. A comparative study was performed to understand and compare the effects of application of stimulation for 3 conditions: The effect of stimulation load without any other loads, the effect of stimulation in presence of the gravity load, and the effect of stimulation in presence of negative pressure. From the results of these simulations, it was established that through the stimulation applied, the tongue movement in the caudal direction is contained for both the negative pressure and gravitational load condition; the soft palate also moves down slightly in the vertical direction; the epiglottis stands up in comparison to its rest condition and moves away from the pharynx wall; and the pharynx wall was stretched. These movements are beneficial for treating the OSA and support the method of ansa cervicalis stimulation. Therefore, this proof-of-concept

study helps lay down the path for a more comprehensive modeling effort for the ACS treatment approaches of OSA.

For the future work, in the automated segmentation using the snake tool, more training data could be used to increase the accuracy and robustness of the automated process. This could be explored in the future. In the OSA study, several limiting assumptions were made for the soft-tissue mechanics model of the airway, especially for the tongue whose movement is a key in the problem. Future works would involve a better way of modeling the nonlinear behavior of the tongue and other components. In addition, defining the contact pairs between the tongue and the soft palate, and also between the tongue and the epiglottis, would help increase the realism of the model.

References

1. Strohl, K. P., Butler, J. P. & Malhotra, A. Mechanical Properties of the Upper Airway. in Comprehensive Physiology (ed. Prakash, Y. S.) 1853–1872 (Wiley, 2012). doi:10.1002/cphy.c110053.
2. Eckert, D. J., Malhotra, A. & Jordan, A. S. Mechanisms of apnea. Prog. Cardiovasc. Dis. 51, 313–323 (2009).
3. Malhotra, A. & White, D. P. Obstructive sleep apnoea. The Lancet 360, 237–245 (2002).
4. Cathain, E. O. & Gaffey, M. M. Upper airway obstruction. in StatPearls [Internet] (StatPearls Publishing, 2022).
5. Martinovits, G., Leventon, G., Goldhammer, Y. & Sadeh, M. Vocal cord paralysis as a presenting sign in the Shy-Drager syndrome. J. Laryngol. Otol. 102, 280–281 (1988).
6. Saboisky, J. P., Chamberlin, N. L. & Malhotra, A. Potential therapeutic targets in obstructive sleep apnoea. Expert Opin. Ther. Targets 13, 795–809 (2009).
7. Li, Z, Wilson, A., Sayce, L., Avhad, A., Rousseau, B., & Luo, H. Numerical and Experimental Investigations on Vocal Fold Approximation in Healthy and Simulated Unilateral Vocal Fold Paralysis. Appl. Sci. 11, 1817 (2021).
8. Nouraei, S. A. R., Middleton, S. E., Butler, C. R. & Sandhu, G. S. An estimation of the population incidence of adult unilateral vocal fold mobility impairment in England. Logoped. Phoniatr. Vocol. 40, 93–94 (2015).
9. Korean Society of Laryngology, Ryu, C.H., Kwon, T.K., Kim, H., Kim, H.S., Park, I.S., Woo, J.H., Lee, S.H., Lim, J.Y., Kim, S.T., Jin, S.M., & Choi, S.H. Guidelines for the Management of Unilateral Vocal Fold Paralysis From the Korean Society of Laryngology, Phoniatrics and Logopedics. Clin. Exp. Otorhinolaryngol. 13, 340–360 (2020).
10. Dailey, S. H. & Ford, C. N. Surgical Management of Sulcus Vocalis and Vocal Fold Scarring. Otolaryngol. Clin. North Am. 39, 23–42 (2006).
11. Bohlender, J. Diagnostic and therapeutic pitfalls in benign vocal fold diseases. GMS Curr. Top. Otorhinolaryngol. - Head Neck Surg. 12Doc01 ISSN 1865-1011 (2013) doi:10.3205/CTO000093.
12. Harries, M. L. Unilateral vocal fold paralysis: a review of the current methods of surgical rehabilitation. J. Laryngol. Otol. 110, 111–116 (1996).
13. Mattioli, F., Bettini, M., Botti, C., Busi, G., Tassi, S., Malagoni, A., Molteni, G., Trebbi, M., Luppi, M.P., Bergami, G., & Pressuti, L. Polydimethylsiloxane Injection Laryngoplasty for Unilateral Vocal Fold Paralysis: Long-Term Results. J. Voice 31, 517.e1-517.e7 (2017).
14. Friedman, A. D., Burns, J. A., Heaton, J. T. & Zeitels, S. M. Early versus late injection medialization for unilateral vocal cord paralysis. The Laryngoscope 120, 2042–2046 (2010).
15. Varadarajan, V., Blumin, J. H. & Bock, J. M. State of the art of laryngeal electromyography. Curr. Otorhinolaryngol. Rep. 1, 171–177 (2013).
16. Hogikyan, N. D., Wodchis, W. P., Terrell, J. E., Bradford, C. R. & Esclamado, R. M. Voice-Related Quality of Life (V-RQOL) following type I thyroplasty for unilateral vocal fold paralysis. J. Voice 14, 378–386 (2000).
17. Siu, J., Tam, S. & Fung, K. A comparison of outcomes in interventions for unilateral vocal fold paralysis: A systematic review: Comparison of Interventions for UVFP. The Laryngoscope 126, 1616–1624 (2016).
18. Benjafield, A. V., Ayas, N.T., Eastwood, P.R., Heinzer, R., Ip, M.S.M, Morell, M.J., Nunez, C.M., Patel S.R., Penzel, T., Pépin, J.L., & Peppard, P.E. Estimation of the global prevalence and burden of obstructive sleep apnoea: a literature-based analysis. Lancet Respir. Med. 7, 687–698 (2019).
19. Yaffe, K., Laffan, A.M., Harrison, S.L., Redline, S., Spira, A.P., Ensrud, K.E., Ancoli-Israel, S., & Stone, K.L. Sleep-Disordered Breathing, Hypoxia, and Risk of Mild Cognitive Impairment and Dementia in Older Women. JAMA 306, (2011).
20. Kushida, C. A., Nichols, D.A., Holmes, T.H., Quan, S.F., Walsh, J.K., Gottlieb, D.J., Simon Jr, R.D., Guilleminault, C., White, D.P., Goodwin, J.L., & Schweitzer, P.K. Effects of Continuous Positive Airway Pressure on Neurocognitive Function in Obstructive Sleep Apnea Patients: The Apnea Positive Pressure Long-term Efficacy Study (APPLES). Sleep 35, 1593–1602 (2012).
21. Marin, J. M., Carrizo, S. J., Vicente, E. & Agusti, A. G. Long-term cardiovascular outcomes in men with obstructive sleep apnoea-hypopnoea with or without treatment with continuous positive airway pressure: an observational study. The Lancet 365, 1046–1053 (2005).
22. Kent, D. T., Zealear, D. & Schwartz, A. R. Ansa Cervicalis Stimulation. Chest 159, 1212–1221 (2021).
23. Kent, D. T. Ansa Cervicalis Stimulation for Obstructive Sleep Apnea. in Upper Airway Stimulation in Obstructive Sleep Apnea (eds. Heiser, C. & De Vries, N.) 293–315 (Springer International Publishing, Cham, 2022). doi:10.1007/978-3-030-89504-4_21.
24. Mansour, K. F., Rowley, J. A. & Badr, M. S. Measurement of pharyngeal cross-sectional area by finite

element analysis. J. Appl. Physiol. 100, 294–303 (2006).
25. Malhotra, A., Huang, Y., Fogel, R.B., Pillar, G., Edwards, J.K., Kikinis, R., Loring, S.H., & White, D.P. The Male Predisposition to Pharyngeal Collapse: Importance of Airway Length. Am. J. Respir. Crit. Care Med. 166, 1388–1395 (2002).
26. Huang, Y., White, D. P. & Malhotra, A. The Impact of Anatomic Manipulations on Pharyngeal Collapse. Chest 128, 1324–1330 (2005).
27. Huang, Y., Malhotra, A. & White, D. P. Computational simulation of human upper airway collapse using a pressure-/state-dependent model of genioglossal muscle contraction under laminar flow conditions. J. Appl. Physiol. 99, 1138–1148 (2005).
28. Avhad, A., Li, Z, Wilson, A., Sayce, L., Chang, S., Rousseau, B., & Luo, H.. Subject-Specific Computational Fluid-Structure Interaction Modeling of Rabbit Vocal Fold Vibration. Fluids 7, 97 (2022).
29. Avhad, A., Wilson, A., Sayce, L., Li, Z., Rousseau, B., Doyle, J.F., & Luo, H. An Integrated Experimental-Computational Study of Vocal Fold Vibration in Type I Thyroplasty. J. Biomech. Eng. 146, 041006 (2024).
30. Li, Z., Wilson, A., Sayce, L., Ding, A., Rousseau, B., & Luo, H. Subject-Specific Modeling of Implant Placement for Type I Thyroplasty Surgery. Ann. Biomed. Eng. 51, 2182–2191 (2023).
31. Faizal, W. M., Ghazali, N.N., Khor, C.Y., Badruddin, I.A., Zainon, M.Z., Yazid, A.A., Ibrahim, N.B., & Razi, R.M. Computational fluid dynamics modelling of human upper airway: A review. Comput. Methods Programs Biomed. 196, 105627 (2020).
32. JeyaJothi, E. S., Anitha, J., Rani, S. & Tiwari, B. A Comprehensive Review: Computational Models for Obstructive Sleep Apnea Detection in Biomedical Applications. BioMed Res. Int. 2022, 1–21 (2022).
33. Pelteret, J. V. & Reddy, B. D. Development of a computational biomechanical model of the human upper-airway soft-tissues toward simulating obstructive sleep apnea. Clin. Anat. 27, 182–200 (2014).
34. Calka, M. et al. Machine-Learning based model order reduction of a biomechanical model of the human tongue. Comput. Methods Programs Biomed. 198, 105786 (2021).
35. Amatoury, J., Kairaitis, K., Wheatley, J. R., Bilston, L. E. & Amis, T. C. Peripharyngeal tissue deformation and stress distributions in response to caudal tracheal displacement: pivotal influence of the hyoid bone? J. Appl. Physiol. 116, 746–756 (2014).
36. Hoffstein, V., Zamel, N. & Phillipson, E. A. Lung Volume Dependence of Pharyngeal Cross-Sectional Area in Patients with Obstructive Sleep Apnea. Am. Rev. Respir. Dis. 130, 175–178 (1984).
37. Rowley, J. A., Permutt, S., Willey, S., Smith, P. L. & Schwartz, A. R. Effect of tracheal and tongue displacement on upper airway airflow dynamics. J. Appl. Physiol. 80, 2171–2178 (1996).
38. Amatoury, J., Cheng, S., Kairaitis, K., Wheatley, J.R., Amis, T.C., & Bilston, L.E. Development and validation of a computational finite element model of the rabbit upper airway: simulations of mandibular advancement and tracheal displacement. J. Appl. Physiol. 120, 743–757 (2016).
39. Cheng, S., Gandevia, S. C., Green, M., Sinkus, R. & Bilston, L. E. Viscoelastic properties of the tongue and soft palate using MR elastography. J. Biomech. 44, 450–454 (2011).
40. Chen, L., Xiao, T. & Ng, C. T. The Biomechanical Mechanism of Upper Airway Collapse in OSAHS Patients Using Clinical Monitoring Data during Natural Sleep. Sensors 21, 7457 (2021).
41. Burd, D. W. Validation of Novel Obstructive Sleep Apnea Treatment with Silicone Gel Experimental Models. (2020) doi:10.34917/23469713.
42. Wang, X., Jiang, W., Zheng, X. & Xue, Q. A computational study of the effects of vocal fold stiffness parameters on voice production. J. Voice 35, 327.e1-327.e11 (2021).
43. Gagnon, C., Boismery, S., Godio-Raboutet, Y., Tuchtan, L., Bartoli, C., Adalian, P., Chaumoitre, K., Piercecchi-Marti, M.D., & Thollon, L. Biomechanical study of the thyroid cartilage: A model of bi-digital strangulation. Forensic Sci. Int. 302, 109891 (2019).
44. Miri, A. K. Mechanical Characterization of Vocal Fold Tissue: A Review Study. J. Voice 28, 657–667 (2014).
45. Luo, H., Scholp, A. & Jiang, J. J. The Finite Element Simulation of the Upper Airway of Patients with Moderate and Severe Obstructive Sleep Apnea Hypopnea Syndrome. BioMed Res. Int. 2017, 1–5 (2017).
46. Carrigy, N. B. et al. Determination Of Passive Pharyngeal Tissue Mechanical Properties Using Finite Element Analysis Simulation. in B60. NEW INSIGHTS IN PATHOPHYSIOLOGY, EPIDEMIOLOGY, AND DETECTION OF SLEEP DISORDERED BREATHING A3546–A3546 (American Thoracic Society, 2015).
47. Hermant, N., Perrier, P. & Payan, Y. Human Tongue Biomechanical Modeling. in Biomechanics of Living Organs 395–411 (Elsevier, 2017). doi:10.1016/B978-0-12-804009-6.00019-5
48. Gerard, J.-M., Wilhelms-Tricarico, R., Perrier, P. & Payan, Y. A 3D dynamical biomechanical tongue model to study speech motor control. (2006) doi:10.48550/ARXIV.PHYSICS/0606148.